

**BILAYER LIGHT-EMITTING ELECTROCHEMICAL CELLS:  
IONIC EFFECTS OF SOLID POLYMER ELECTROLYTE**

by

Chaobei Tong

A thesis submitted to the  
Department of Physics, Engineering Physics and Astronomy  
In conformity with the requirements for  
the degree of Master of Science

Queen's University  
Kingston, Ontario, Canada  
(August 2022)

Copyright © Chaobei Tong, 2022

## Abstract

Polymer light-emitting electrochemical cells (PLECs) are organic solid-state devices that operate on *in situ* electrochemical doping and the formation of a light-emitting p-n junction. Bilayer LECs consist of a solid polymer electrolyte (SPE) underlayer and a conjugated polymer (CP) top layer. Aluminium electrodes with 2mm gap size were deposited on top of the CP layer and formed a planar configuration. Planar bilayer LECs with large gap sizes brought unique opportunities to visualize the *in situ* doping propagations with imaging techniques. Separating the CP from the SPE provided the potential to study the SPE layer itself and lead to a better performing light emitting device. In this thesis, four different studies were conducted to explore ionic transportation in the CP, the SPE, and the CP/SPE interface. In the study of salt concentrations in the SPE, the increase in ionic concentrations improved the performance of LECs in terms of doping propagation speed, junction formation time, and cell current. However, a current leveling off was observed at high salt concentrations, while light emitting p-n junction overlaps with the cathode which is undesirable. In the second study, by increasing SPE layer thickness, a significant improvement in device performance was observed, however, no further improvement was observed as the thickness went beyond 500nm. In the study of cationic effects, devices with smaller cation sizes had a higher current and faster doping propagation, whereas devices with large cations require a higher bias voltage and temperature to turn on. The improved performance of bilayer LECs compared to single-layer LECs suggested that interlayer ionic transportation was not the major factor that limited the performance of LECs. In the final chapter, LECs with salt concentrations as low as 0.005 were successfully turned on. For devices with lower salt concentrations, however, no light-emitting p-n junction was formed. These

studies demonstrate the importance of ion transport in LEC operation and point to new directions for improving the device performance.

## **Co-authorship**

The results in Chapter 4 and Chapter 5 have been published in *Electrochimica Acta*, Volume 423, 2022, 140574, ISSN 0013-4686, which have the following co-authors: Abhishake Goyal, Dongze Wang, and Professor Jun Gao. The contribution of co-authors, Abhishake Goyal and Dongze Wang was primarily through the participation in device fabrication and providing insightful ideas. Professor Jun Gao provided the supervision, conceptualization, reviewing and editing of the writing.

## Acknowledgements

I want to take this opportunity to thank everyone who nurtures me along the way during my Master of Science degree. Without the exceptional support of my supervisor, Professor Jun Gao, this thesis will not be achievable. Thank you, Professor Gao, for your ongoing guidance and generosity. I appreciate your going above and beyond to empower me during my time in your research group. I am grateful for this amazing journey at Queen's University.

Moreover, I would like to thank my colleague and group members for their feedback and insights throughout my research projects. Thank you, Dongze Wang, Abhishake Goyal, Dr. Shiyu Hu, Kiran Birdee, and Huang Wei (Laurence) Yeh.

It is a pleasure to be a member of the CREATE-MAPS program. Shoutout to James Fraser for the workshops and opportunities. With the COVID-19 pandemic, I was faced with many challenges. However, with the support of the Department of Physics, I was able to conquer obstacles and drive with adverse mindsets.

Last but not the least, I want to thank my family and friends. Thank you, my beloved girlfriend, Grace Zhou for walking and being by my side. For laughing with joy and crying with me through my pain. I appreciate all your encouragement. You are my sunshine over the rain. I am grateful for the peer support, edits, and comments you provided to me.

To my one and only cat, Melody, thank you for accompanying me. I cannot ask for any better joy through my unbroken words. Thank you, my grandparents and parents, Yiling Tong, Shuzhen Zhao, Shijie Tong, and Lin Ma, for their longing and exception. Thank you for the invaluable advice and unconditional love of who I am. For providing me with all I ever needed. Be brave and achieve my dream. Never give up like strong armor.

## Table of Contents

Abstract .....	ii
Co-authorship.....	iv
Acknowledgements.....	v
List of Figures.....	viii
List of Tables .....	xi
List of Abbreviations .....	xii
Chapter 1 Introduction .....	1
1.1 Background.....	1
1.2 Light-Emitting Electrochemical Cells .....	3
1.3 Bilayer Light-Emitting Electrochemical Cells.....	5
1.4 Scope.....	9
Chapter 2 Motivation and Objectives .....	10
2.1 Motivation.....	10
2.2 Objectives .....	11
Chapter 3 Methodology .....	12
3.1 Materials and Device Fabrication .....	12
3.1.1 Materials .....	13
3.1.2 Solution Preparation.....	14
3.1.2.1 Modifying Salt Concentration.....	14
3.1.2.2 Modifying Thickness of SPE Layer.....	14
3.1.2.3 SPE Solutions with Different Cations.....	15
3.1.2.4 SPE Solutions with Extreme Low Salt Concentration.....	15
3.1.3 Thin Polymer Films .....	16
3.1.4 Electrodes Depositions.....	16
3.2 Device Testing .....	19
3.2.1 Probe Station.....	19
3.2.2 Thickness Measurements .....	20
Chapter 4 Effects of Salt Concentration .....	21
4.1 Introduction.....	21
4.2 Result and Discussion .....	22
4.3 Conclusion .....	33
Chapter 5 Effects of SPE Layer Thickness .....	34

5.1 Introduction.....	34
5.2 Result and Discussion .....	35
5.3 Conclusion .....	39
Chapter 6 Effects of Cation.....	40
6.1 Introduction.....	40
6.2 Result and Discussion .....	41
6.2.1 Alkali Metals.....	41
6.2.2 Transition Metals .....	48
6.2.3 Ammonium .....	51
6.3 Conclusion .....	56
Chapter 7 Extremely Low Salt Concentration Devices .....	57
7.1 Introduction.....	57
7.2 Result and Discussion .....	58
7.3 Conclusion .....	70
Chapter 8 Conclusion.....	72
8.1 Conclusion .....	72
8.2 Future Work.....	75
Appendix A Finding Junction Formation Time .....	77
Method 1: Time-Lapsed Images .....	77
Method 2: Fitting Current vs. Time Curve .....	78
Appendix B Finding Average p-doing Speed.....	79
References.....	80

## List of Figures

Figure 1.1 Schematic for different LEC configurations. (a) Sandwich LEC (b) Planar LEC.....	3
Figure 1.2 A schematic of bilayer planar LEC, which consists of a conjugated polymer top layer and a solid polymer electrolyte underlayer.....	6
Figure 1.3 Schematic cross-sectional operation mechanism of bilayer LECs. (a) Bilayer LECs without any bias voltage. The mobile ions are randomly distributed in the SPE layer. (b) After applying a sufficient bias voltage, mobile ions enter the CP layer to compensate for the injected charges. (c) Narrow light-emitting p-n junction formed when the p-doping front made contact with the n-doping front. ....	7
Figure 3.1 MBraun inert atmosphere glovebox/evaporator system. ....	12
Figure 3.2 Fume hood. ....	13
Figure 3.3 BOC Edwards AUTO500 Vacuum Chamber inside of the glovebox. ....	17
Figure 3.4 Shadow mask for four substrates with three electrodes of 2mm gap size. ....	18
Figure 3.5 Janis ST-500 micro-manipulated probe station set up.....	20
Figure 4.1 A MEH-PPV/PEO:KOTf bilayer LEC tested under a constant bias voltage of 25V and a constant temperature of 330K. The images were captured under the illumination of a 365nm UV ring light from above. ....	23
Figure 4.2 Cell Current as a function of time for LEC devices with different salt concentrations tested under a constant bias voltage of 25V and a constant temperature of 330K. ....	24
Figure 4.3 Initial and peak current as a function of salt concentration under a constant bias voltage of 25V and a constant temperature of 330K. ....	25
Figure 4.4 Junction formation time as a function of salt concentration. The junction formation time was determined from current vs. time characteristics and the time-lapsed images and presented in red and blue, respectively. The methods for determining the junction formation times were described in Appendix A.....	27
Figure 4.5 Average p-doping position from anode as a function of time determined from the time-lapsed images. ....	28
Figure 4.6 p-doping propagation speed as a function of salt concentration. The average p-doping speed was determined as described in Appendix B. ....	29
Figure 4.7 (a)-(f) Images taken at peak current for LECs with different salt concentrations. (g) Average junction position relative to the anode as a function of salt concentration. ....	31
Figure 4.8 (a) PL image showing a typical doping profile before junction formation. (b) A schematic showing the cross-section of bilayer cell before junction formation. ....	33

Figure 5.1 Cell Current as a function of time for LEC devices with different SPE layer thickness tested under a constant bias voltage of 15V and a constant temperature of 330K. ....	35
Figure 5.2 Junction formation time as a function of SPE layer thickness. The junction formation times were determined from the current vs. time curves as described in Appendix A. ....	36
Figure 5.3 Initial cell current as a function of SPE layer thickness. ....	37
Figure 5.4 Average p-doping speed as a function of SPE layer thickness. The average p-doping speed was determined as described in Appendix B. ....	38
Figure 5.5 Time-lapsed images captured for bilayer LECs with SPE layer thickness of 770 nm and 500 nm. ....	39
Figure 6.1 Current vs time characteristics for MEH-PPV/PEO/LiClO <sub>4</sub> bilayer LEC tested under a constant bias voltage of 25V and a constant temperature of 330K. (a)-(h) Time lapsed images captured under the illumination of a 365nm UV ring light from above. ....	42
Figure 6.2 Cell Current as a function of time for LEC devices with different alkali metal cations tested under a constant bias voltage of 25V and a constant temperature of 330K. ....	43
Figure 6.3 Junction formation time as a function of cation radius. The junction formation time was determined from current vs. time characteristics and the time-lapsed images and presented in red and blue, respectively. The methods for determining the junction formation times were described in Appendix A. ....	44
Figure 6.4 Initial current as a function of cation radius under a constant bias voltage of 25V and a constant temperature of 330K. ....	45
Figure 6.5 Images captured at peak current for LECs devices with (a) Li salt (b) Na salt (c) K salt (d) Cs salt. ....	46
Figure 6.6 The normalized junction position at peak current (relative to anode) as a function of cation radius. Bilayer data were extracted from the time-lapsed images of devices with 2mm gap size. Single layer data were taken from devices with gap size of 11mm. [46]. ....	47
Figure 6.7 Time-Lapsed images for bilayer LEC device with ZnOTf salt tested under a constant bias voltage of 100V and a constant temperature of 360K. ....	49
Figure 6.8 Time-Lapsed images for bilayer LEC device with EuOTf salt tested under a constant bias voltage of 100V and a constant temperature of 360K. ....	50
Figure 6.9 Time-Lapsed images for bilayer LEC device with AmOTf salt tested under a constant bias voltage of 25V and a constant temperature of 330K. ....	51
Figure 6.10 Time-Lapsed images for single layer LEC device with AmOTf salt tested under a constant bias voltage of 25V and a constant temperature of 330K. (a)-(d) captured under the illumination of a 365nm UV ring light from above. (e) captured with no additional light source. ....	52

Figure 6.11 Cell Current as a function of time for single layer and bilayer LEC devices with AmOTf salt tested under a constant bias voltage of 25V and a constant temperature of 330K..... 54

Figure 6.12 Cell Current as a function of time for bilayer LEC devices with AmOTf and KOTf salt tested under a constant bias voltage of 25V and a constant temperature of 330K. .... 55

Figure 7.1 Images captured at peak current for 2mm bilayer LECs devices with ..... 58

Figure 7.2 Cell Current as a function of time for LEC devices with 100:1 and 200:1 PEO:KOTf concentration tested under a constant bias voltage of 50V and 100V and a constant temperature of 360K. .... 60

Figure 7.3 Images captured once the doping propagation stopped for LECs devices with PEO: KOTf concentrations of 400:1 under a constant temperature of 360K and a constant bias voltage of (a) 100V (b) 200V (c) 400V (d) 800V..... 62

Figure 7.4 Final p-doping front position relative to the anode as a function of bias voltage for 2mm bilayer LECs with PEO: KOTf concentration of 400:1..... 63

Figure 7.5 Cell Current as a function of time for LEC devices with 400:1 PEO:KOTf concentration tested under different constant bias voltage and a constant temperature of 360K. .... 64

Figure 7.6 Initial p-doping speed as a function of bias voltage for 2mm bilayer LECs with PEO: KOTf concentration of 400:1. .... 65

Figure 7.7 Cell Current as a function of time for LEC devices with K and Na salts tested under a constant bias voltage of 800V and a constant temperature of 360K. The PEO:Salt concentrations were 400:1. .... 66

Figure 7.8 Images captured once the doping propagation stopped for LECs devices with PEO: Salt concentrations of 400:1 under a constant temperature of 360K and a constant bias voltage of 800V. (a) Device with potassium salt. (b) Device with sodium salt. .... 67

Figure 7.9 Images captured at peak current for single layer and bilayer LEC devices with PEO: Salt concentrations of 25:1 (a) Single layer LEC tested under a constant temperature of 330K and a constant bias voltage of 25V (b) Single layer LEC tested under a constant temperature of 360K and a constant bias voltage of 25V. (c) Single layer LEC tested under a constant temperature of 360K and a constant bias voltage of 200V. (d) Bilayer LEC tested under a constant temperature of 330K and a constant bias voltage of 25V. .... 69

## List of Tables

Table 5.1 Thickness of SPE layer by varying initial spin speed and solution dilution factor.....	34
Table 7.1 Initial current, peak current, junction formation time and junction position as a distance from the anode for bilayer LEC devices with different PEO:KOTf concentrations and tested under different bias voltage. The junction formation times were determined from current vs. time curves as described in Appendix A.....	61

## List of Abbreviations

<b>AmOTf</b>	Ammonium Trifluoromethanesulfonate
<b>CP</b>	Conjugated Polymer
<b>CsClO<sub>4</sub></b>	Cesium Perchlorate
<b>EC</b>	Ethylene Carbonate
<b>EL</b>	Electroluminescence
<b>EuOTf</b>	Europium Trifluoromethanesulfonate
<b>KClO<sub>4</sub></b>	Potassium Perchlorate
<b>KOTf</b>	Potassium Trifluoromethanesulfonate
<b>LEC</b>	Light-Emitting Electrochemical Cell
<b>LiClO<sub>4</sub></b>	Lithium Perchlorate
<b>MEH-PPV</b>	Poly[2-methoxy-5-(2-ethylhexyloxy)-1,4-phenylenevinylene]
<b>NaClO<sub>4</sub></b>	Sodium Perchlorate
<b>OTf</b>	Trifluoromethanesulfonate
<b>PEO</b>	Poly(ethylene oxide)
<b>PL</b>	Photoluminescence
<b>PPC</b>	Polypropylene Carbonate
<b>PVD</b>	Physical vapor deposition
<b>SPE</b>	Solid Polymer Electrode
<b>TbOTf</b>	Terbium Trifluoromethanesulfonate
<b>w/v %</b>	Weight vs. Volume Percentage
<b>ZnOTf</b>	Zinc Trifluoromethanesulfonate

# Chapter 1

## Introduction

### 1.1 Background

Electroluminescence (EL) is the generation of light by the electrical excitation of light-emitting phosphors. The phenomenon was first reported by Henry Round in 1907 when current passed through a silicon carbide crystal. [1][2] In 1936, George Destriau observed the emission of light from zinc sulfide (ZnS) under applied voltage. [3] EL produced in organic fluorescent compounds was first reported by A. Bernanose in 1953, when high alternating voltages were applied to acridine derivatives such as gonacrin (I) and acridine orange E (II). [4]

The significant breakthrough of organic EL devices occurred in 1987. Tang and VanSlyke reported the first organic light-emitting diode (OLED) with an organic heterojunction structure. Light emission was observed with a forward bias as low as about 2.5V, whereas the diode has high electroluminescent emission efficiency and fast response. [5] In 1990, J. H. Burroughes introduced the first light-emitting diodes based on conjugated polymers. The structural, mechanical, and processing properties of polymers brought unique advantages to thin film fabrication and provided the potential for the development of large-area light-emitting displays. [6]

An alternative approach to achieving organic electroluminescence was discovered by Qibing Pei in 1995 in what is known as the light-emitting electrochemical cells (LECs). [7] The introduction of mobile ions in LECs leads to the electrochemical p-doping and n-doping of the light emitters and the formation of a p-n junction where

electroluminescence can be observed. By introducing mobile ions into the organic semiconductor, the device can have a simpler structure with a single organic layer consisting of a conjugated polymer and a polymer electrolyte. The thickness of the polymer layer is less critical which makes it possible to use a variety of substrates such as clothing, paper, or complicated shapes like kitchen forks. [8][9][10] However, the LECs still lag in operational lifetime, efficiency, and stability. Therefore, it is critical to investigate and understand the many factors that affect the LEC operation and performance.

## 1.2 Light-Emitting Electrochemical Cells

Light-emitting electrochemical cells (LECs) are solid-state electroluminescent devices that operate on redox doping reactions involving the transport of both ionic and electronic charges. [7][11] The structure of LECs can be similar to organic light-emitting diodes (OLEDs), where the light emitters can be luminescent conjugate polymers (CPs). [12][13] The introduction of mobile ions in LECs leads to electrochemical p-doping and n-doping of the light emitters and the formation of a p-n junction where electroluminescence can be observed. Typically, there are two different configurations of LEC as shown in Figure 1.1.

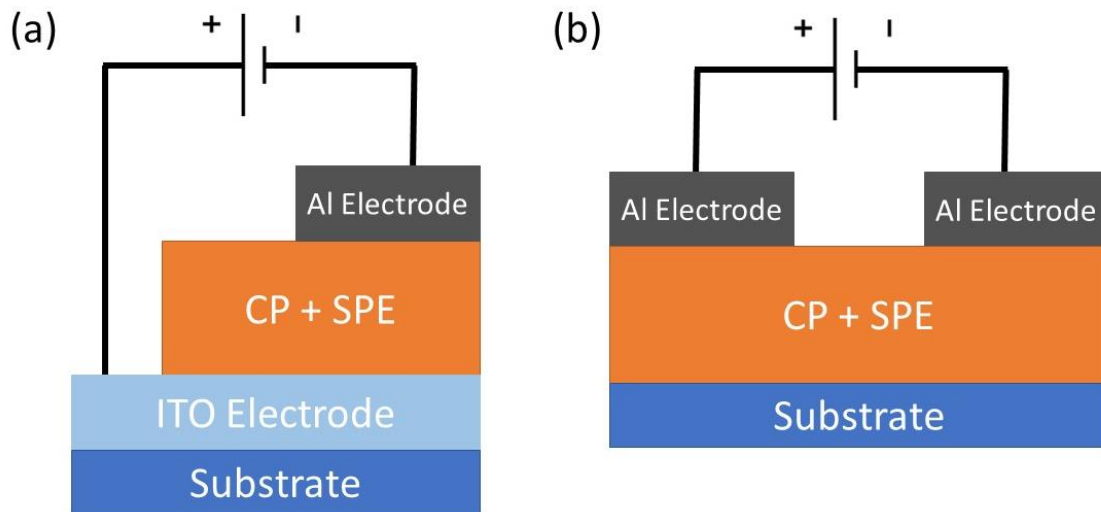


**Figure 1.1 Schematic for different LEC configurations. (a) Sandwich LEC (b) Planar LEC**

Figure 1.1(a) shows the sandwich configuration of LEC. The active layer which consists of conjugated polymer and solid polymer electrolyte is sandwiched between two electrodes. One of the electrodes could be metal such as aluminum, while the other

electrode is made of a transparent ITO material. Once sufficient current pass through the active layer, EL could be observed through the ITO electrode.

The planar configuration, as shown in Figure 1.1(b), has both electrodes deposited on top of the polymer active layer. As p-doped and n-doped regions propagated from anode and cathode, respectively, the doping fronts eventually meet to form a p-n junction, where EL can be observed in a narrow region. This planar bilayer LEC configuration has been widely used to study the dynamic doping process on single-layer devices because it allows for the visualization of the doping process and junction location. [14][15][16]

### 1.3 Bilayer Light-Emitting Electrochemical Cells

Mixing light-emitting CPs and solid polymer electrolyte (SPE) can be challenging. Non-polar CPs is not compatible with polar electrolyte, which means they cannot co-dissolve in a common solvent. Researchers have developed multiple methods to improve the phase morphologies of the polymer composites, such as thermal annealing [17], a surfactant-like additive [18], crown-ether, ionic-liquid-based electrolytes [19][20], or the introduction of bifunctional polymers that possess both ionically and electronically conductive moieties [21][22][23]. A notable alternative option is the ionic transition-metal complex (iTMC)-based LECs, where ionic salt is replaced by ionic species. [24][25] However, the addition of ionic salt is still required for high-performance devices because of the poor ionic conductivities of iTMCs. [26][27][28] Another approach is the salt-doped LECs which only contains a molecular salt, such as lithium triflate, without any electrolyte polymer, but these devices always require a high voltage to activate.[29][30]

The problem of mixing CPs and SPEs was completely circumvented with a bilayer planar structure first introduced in 2010. [31] The bilayer planar LECs were fabricated on glass substrates, onto which Au electrodes were deposited. The bilayer structure was formed by first spin coating a yellow-emitting conjugated polymer layer, then followed by the spin coating of the electrolyte on top. The electrodes have a 300 $\mu$ m gap between their inner edges, which was smaller than the gap sizes typically used in our group.

Figure 1.2 shows the schematic of bilayer LECs that was used in my thesis studies. The underlying SPE layer consists of a mixture of PEO and salt. MEH-PPV was selected as the top conjugated polymer layer. Aluminum electrodes were deposited on top of the

polymer layer and the gap size between the electrodes was 2mm. The large gap size between the electrodes made it easier to visualize the *in situ* doping propagations with time-lapsed imaging techniques.

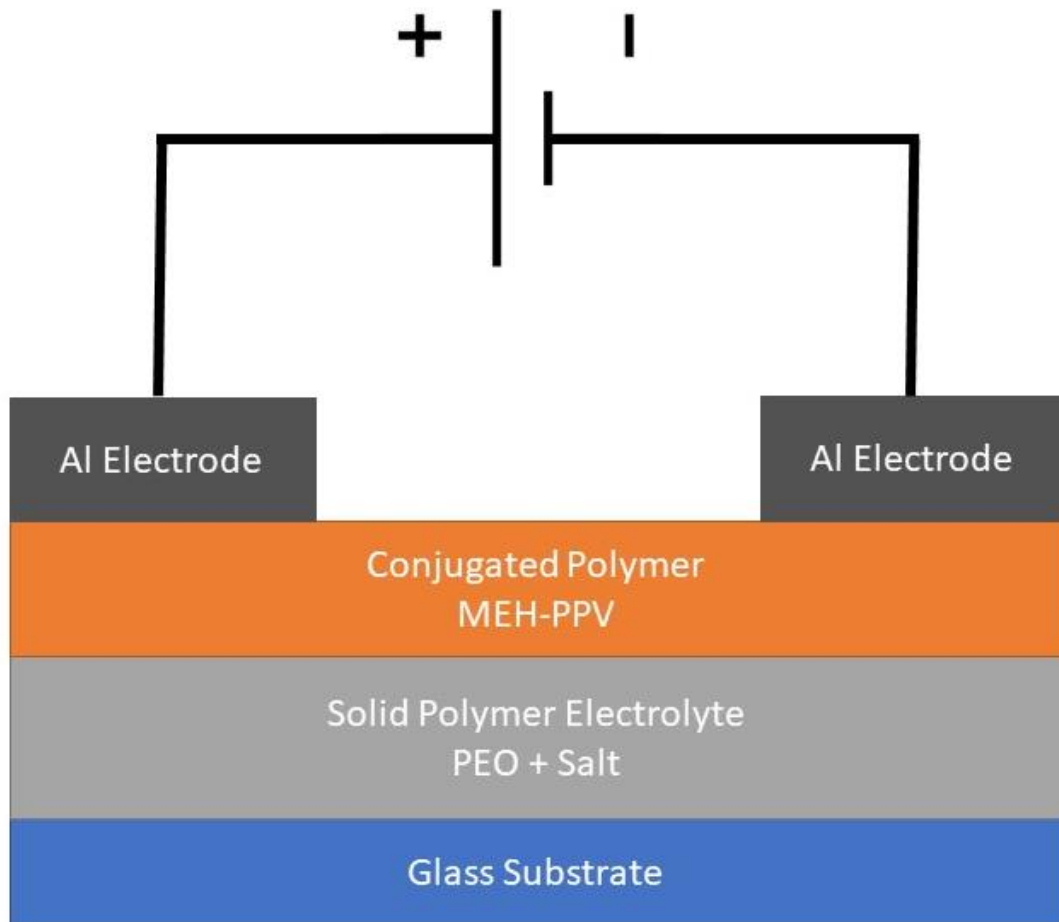


**Figure 1.2** A schematic of bilayer planar LEC, which consists of a conjugated polymer top layer and a solid polymer electrolyte underlayer.

Before applying any bias voltage, mobile ions are randomly distributed in the SPE layer. Under a sufficient bias voltage, electrons and holes are injected from the cathode and anode to the CP respectively. Mobile ions enter the CP to compensate for the injected charges, which causes the doping of the CP. With a sufficient doping current, the p-doping front start to propagate from the positively biased anode, while the n-doping front start to propagate from the negative bias anode. As the doping fronts continue to grow toward the opposite electrode, p-doping and n-doping fronts meet and form a light emitting p-n junction where EL can be observed from a narrow region.

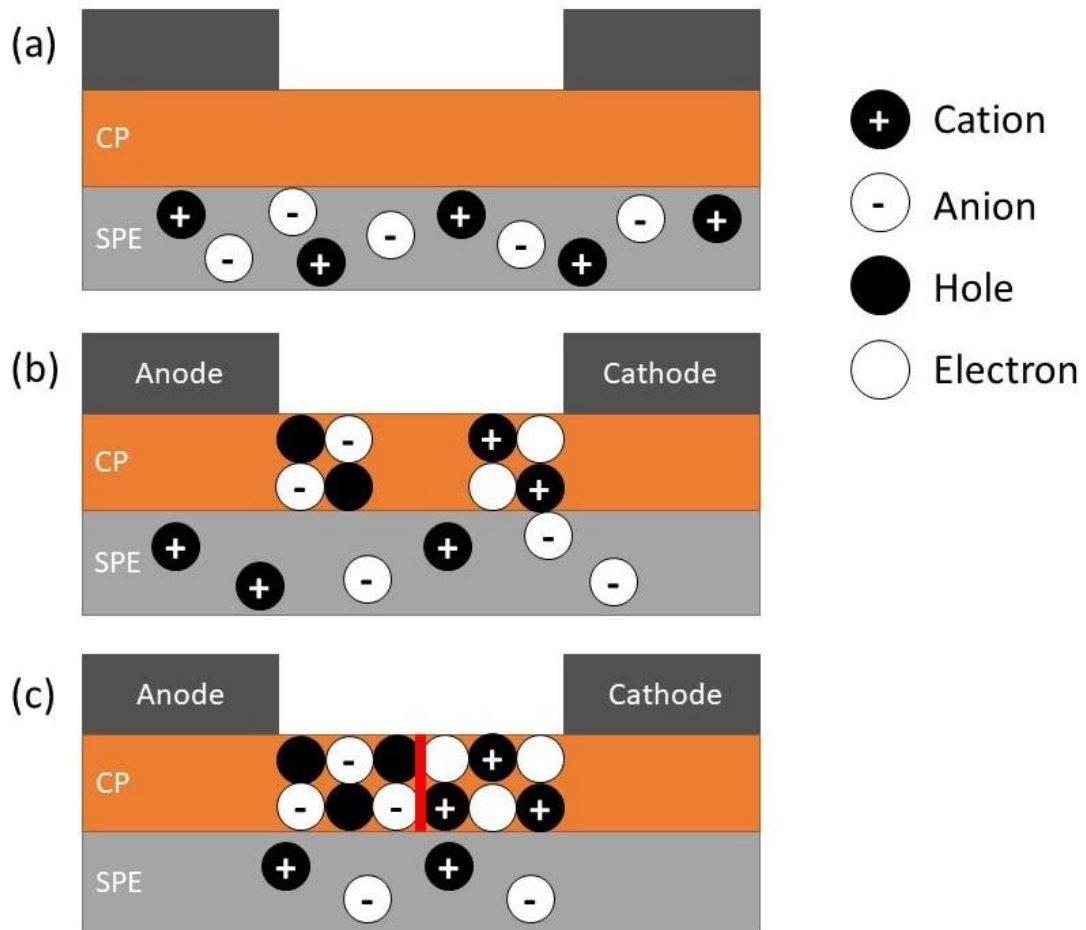


**Figure 1.3 Schematic cross-sectional operation mechanism of bilayer LECs. (a) Bilayer LECs without any bias voltage. The mobile ions are randomly distributed in**

**the SPE layer. (b) After applying a sufficient bias voltage, mobile ions enter the CP layer to compensate for the injected charges. (c) Narrow light-emitting p-n junction formed when the p-doping front made contact with the n-doping front.**

## **1.4 Scope**

The thesis consists of the following 8 chapters:

Chapter 1, the current chapter, introduced light-emitting electrochemical cells, especially bilayer planar light-emitting electrochemical cells.

Chapter 2 introduced the motivation and objectives of the studies on bilayer planar LECs.

Chapter 3 provided step-by-step procedures for device fabrication and device testing.

Chapter 4 presented the experimental data and discussions on the effects of salt concentration on planar bilayer LECs.

Chapter 5 presented the effects of SPE layer thickness on planar bilayer LECs.

Chapter 6 discussed the effects of cation by comparing planar LECs fabricated from different salts.

Chapter 7 continued the studies in Chapter 4, which focused on planar LECs with extremely low salt concentrations.

Chapter 8 provided a summary and an outlook for future work on bilayer LECs.

## Chapter 2

### Motivation and Objectives

#### 2.1 Motivation

A previous study of our group demonstrated large bilayer planar LECs, which allowed the dynamic doping process to be imaged in detail. Our result provided direct evidence that the doping in these bilayer cells is limited by the ionic resistance of the underlying SPE layer. [32] Important questions remain as to how the salt concentration in the SPE layer will affect the ionic resistance. The salt concentration effects in single-layer mixed conductor LECs were investigated in earlier studies, which suggested that an increase in ion concentration results in an increased conductivity of an active layer. [33][34]

However, there are no such data available on how the salt concentration will affect the behaviors of bilayer cells, and how deep in the SPE underlayer will the ions be involved in the doping propagation. Separating the SPE layer from the CP provided opportunities to separately optimizing the layers. In my thesis study, I have also investigated the effects of salt cation types and successfully turned on LECs with record low salt concentrations. We found that the junction position is more centered for devices with low salt concentrations.

## **2.2 Objectives**

In this thesis, the effect of salt concentration, SPE layer thickness, and cation type in bilayer planar LECs will be investigated under constant bias voltage and constant temperature. The doping process will be visualized with imaging techniques, and the performance of the devices, including doping propagation speed, junction formation time, cell current, and junction position, will be presented. The purpose of these studies is to investigate the role of mobile ions in LECs and determine the limitations of ionic concentrations and mobilities. These studies can potentially lead to a high-performance light-emitting devices and also provided unique opportunities to study the solid polymer electrolyte itself.

## Chapter 3

### Methodology

All the fabrication and testing procedures are strictly following the techniques developed by other members in the group.

#### 3.1 Materials and Device Fabrication

All LEC devices were fabricated in an MBraun inert atmosphere glovebox/evaporator system, which is filled with dry nitrogen, as shown in Figure 3.1. All glassware and substrates were prepared in the fume hood as shown in Figure 3.2.



**Figure 3.1 MBraun inert atmosphere glovebox/evaporator system.**



**Figure 3.2 Fume hood.**

### **3.1.1 Materials**

The luminescent conjugate polymer used in these studies was the red-emitting poly[2-methoxy-5-(2-ethylhexyloxy)-1,4-phenylenevinylene] (MEH-PPV), sourced from OLEDKing Optoelectronic Materials Ltd, China. Poly(ethylene oxide) (PEO,  $M_w=2M$ ) was purchased from Sigma Aldrich. Salts that were utilized in the electrolytes include potassium trifluoromethanesulfonate (KOTf), lithium perchlorate ( $LiClO_4$ ), sodium perchlorate ( $NaClO_4$ ), potassium perchlorate ( $KClO_4$ ), cesium perchlorate ( $CsClO_4$ ), europium trifluoromethanesulfonate (EuOTf), terbium trifluoromethanesulfonate (TbOTf), zinc trifluoromethanesulfonate (ZnOTf), ammonium trifluoromethanesulfonate (AmOTf), were purchased from Sigma Aldrich and used as received.

### 3.1.2 Solution Preparation

MEH-PPV was dissolved in toluene, with concentration (in w/v %) of 0.5%, which is 5 mg of MEH-PPV dissolved per 1 mL of toluene solvent. PEO and salt with different weight ratios were dissolved and mixed in cyclohexanone. The solutions were stirred and heated to 60°C on a hot plate until fully dissolved and cooled to room temperature before casting the polymer films.

#### 3.1.2.1 Modifying Salt Concentration

In the study on the salt concentration effects of the SPE layer, PEO and KOTf were dissolved separately in cyclohexanone with concentrations (in w/v%) of 2% and 5%, respectively. Different amounts of PEO and KOTf solutions were mixed to make SPE solutions with KOTf: PEO weight ratios of 0.4, 0.2, 0.13, 0.1, 0.04, 0.025, 0.0125.

Different volume of cyclohexanone was added into each solution to ensure the solutions have the same amount of solvent. This prevents any thickness variation between films upon the cast of the thin SPE films.

#### 3.1.2.2 Modifying Thickness of SPE Layer

To study the effects of the SPE layer thickness, the solutions with KOTf: PEO weight ratio of 0.13 were utilized. To modify the thickness of the SPE layers, the solution was diluted with cyclohexanone by a factor of two and three, respectively.

### 3.1.2.3 SPE Solutions with Different Cations

To analyze the effect of cations, the SPE solutions made with different salts were directly dissolved in 2% PEO/cyclohexanone solutions. These solutions were made with the same molar ratio:  $5 \times 10^{-5}$  moles of cations dissolved in 1mL of 2% PEO/cyclohexanone (in w/v%) solution. The solutions were stirred and heated at a temperature of 80°C on a hot plate until the salts were fully dissolved.

### 3.1.2.4 SPE Solutions with Extreme Low Salt Concentration

SPE solutions with extremely low salt concentrations were achieved by first mixing 2% PEO and 1% KOTf (in w/v%) cyclohexanone solutions to create SPE solution with 0.01 KOTf: PEO weight ratios. This solution was diluted by 2% PEO/cyclohexanone (in w/v%) into solutions of 0.005, 0.0025, 0.00125 KOTf: PEO weight ratio.

### **3.1.3 Thin Polymer Films**

15 mm square glass slides, with a thickness of 1 mm were used as substrates to prepare polymer films. Ultrasonic baths filled with distilled water, acetone, and isopropyl, respectively, were utilized to clean the substrates. Afterward, the substrates were treated with UV-ozone to remove organic residuals. The thin polymer films were cast on the glass substrates with a Chemat Technology KW-4A spin coater. The bilayer structure was formed by first spin coating the SPE layer on the substrate and then followed by the casting of the light-emitting CP layer on top. For each layer, 200 $\mu$ L of the solution was deposited and spun at an initial speed of 2000 RPM for 60 seconds to determine the thickness of the film, and then followed by 4000 RPM for 120 seconds to dry the film. (Note that for the thickness effect study, the initial spin speed for the SPE layer was modified to achieve a different thickness). Each film was baked on a hot plate at 50°C for at least 5 hours to ensure the solvent was completely evaporated. If the devices need to be tested below the melting temperature of PEO, then thermal annealing should be performed. The polymer films were baked at 130°C for 10 minutes, then immediately transferred onto a copper block to cool down.

### **3.1.4 Electrodes Depositions**

A BOC Edwards AUTO500 thermal evaporator was used to deposit aluminum electrodes on top of the polymer films via physical vapor deposition (PVD). The PVD system is located inside the glove box to protect the polymer films from exposure to oxygen or water. The deposition processes were taken place in a vacuum chamber as shown in Figure 3.3.

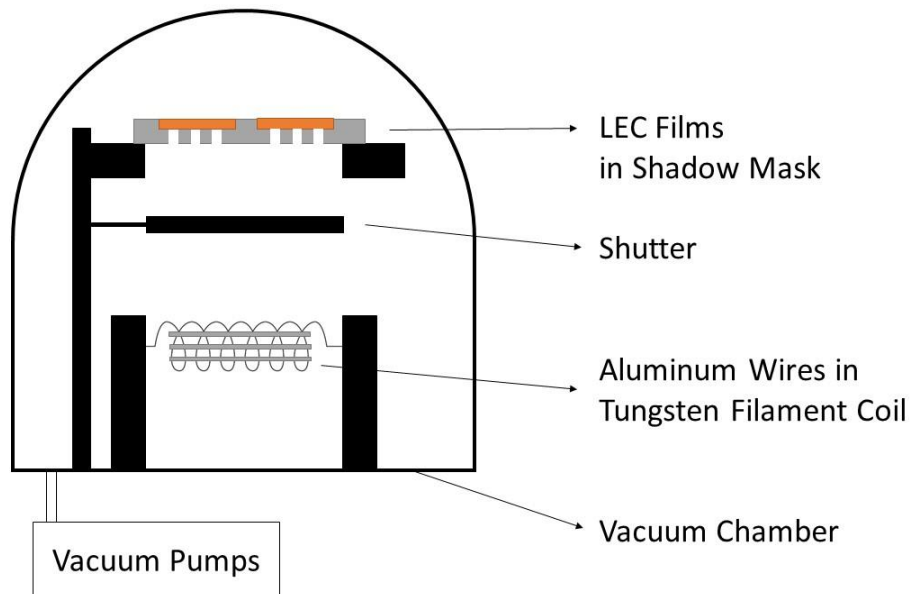


**Figure 3.3 BOC Edwards AUTO500 Vacuum Chamber inside of the glovebox.**

Aluminum wires were cut and loaded into a tungsten filament coil. The polymer films were placed into a shadow mask as shown in Figure 3.4. The shadow mask had four substrate slots, which allowed the electrodes to be deposited onto four films simultaneously. Each slot had three electrode cutouts with gap sizes of 2mm, which made two LEC devices on the same film.

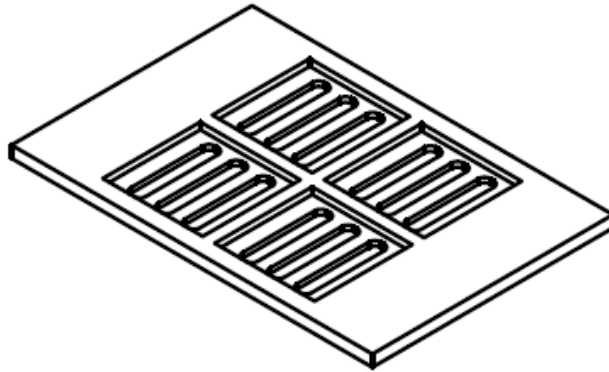


**Figure 3.4 Shadow mask for four substrates with three electrodes of 2mm gap size.**

Before initiating the deposition process, the pressure inside the vacuum chamber was evacuated to  $2 \times 10^{-6}$  Torr with a vapor diffusion pump and a BOC Edwards RV 12 Rotary Vane Pump. The current across the tungsten filament coil was manually increased gradually until the aluminum was vaporized and reached a steady deposition rate of 0.1nm/s. The shutter was opened, and aluminum was deposited onto the exposed regions of the shadow mask until the thickness of the electrode reached a thickness of 100nm.

## **3.2 Device Testing**

### **3.2.1 Probe Station**

The finished devices were transferred into a Janis ST-500 micro-manipulated probe station as shown in Figure 3.5. The edges and the back of the substrates were cleaned using cotton swabs to avoid any shortage between the LEC devices and the station. The LECs devices were placed on top of the gold-plated sample stage. Thermal paste was applied between the device and the sample stage to ensure a suitable thermal contact and reduce the reflection from the sample stage. Indium metal balls were attached to the tip of the probe arm pin. The soft and conductive indium metal balls protect the LEC devices from being scratched and ensure stable connections. A LabVIEW-controlled Keithley 237 source measurement unit was used to apply a constant bias voltage to the cells and simultaneously measure the resulting cell current. A UV ring light was positioned on top of the vacuum chamber window to provide illumination to image the photoluminescence of the films. A computer-controlled Nikon D300 Digital camera with a macro lens was used to capture images.

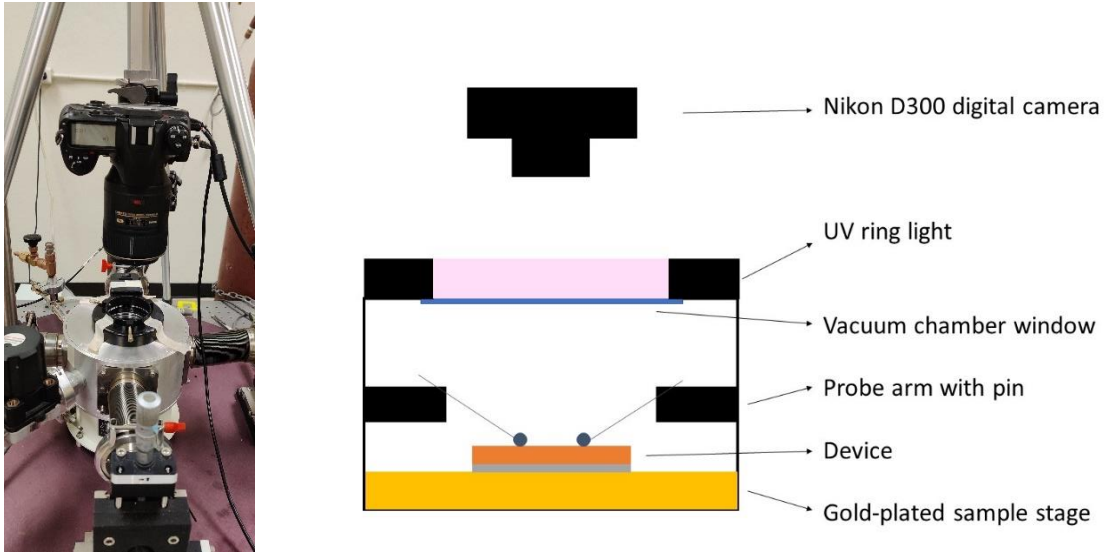


**Figure 3.5 Janis ST-500 micro-manipulated probe station set up.**

Before conducting tests on the LEC device, the vacuum chamber was evacuated to  $10^{-5}$  Torr using a turbo pump. The devices were heated to the designated temperature by a Cryo Con 32B Temperature Controller. The probe arms were lowered to make contact with the electrodes to initiate the test once the pressure and the temperature were stable.

### 3.2.2 Thickness Measurements

The polymer film thickness was measured with a Dektak stylus profiler. The area in between two electrodes was scratched by using the back of a blade. As a result, the polymer films were completely removed without damaging the glass substrate. The stylus probe of the profilometer traveled perpendicular to the scratches. The thickness of the polymer films was determined by measuring the depth of the scratches. This process was repeated at least five times to calculate the average thickness of the films.

## Chapter 4

### Effects of Salt Concentration

#### 4.1 Introduction

Mobile ions play critical roles in the operation of LECs. The doping of the CP occurs with the insertion of the mobile ions from the electrolyte once the bias voltage is applied. The existence of mobile ions improves the conductivity of the undoped regions which helps to sustain a sufficient cell current which leads to doping propagation until junction formation. Therefore, it is important to study the effects of salt concentration in LECs. For sandwich LECs, high-performance LECs typically require a very low electrolyte content to optimize operational lifetime. [35][36][37] A notable exception is LECs made with silver salt. [38] Large planar LECs have advantages to visualize the effect of salt concentration, however, the experimental data for such studies are still lacking. Early studies suggested that planar LECs could not form light-emitting p-n junctions if the salt concentration is below a critical value. [39][40] However, such studies did not provide a complete picture of how salt concentration could affect the doping propagation, cell current, and junction formation. In this chapter, bilayer LECs with salt concentration (in weight ratio) from 0.4 to 0.0125 were demonstrated and discussed.

## 4.2 Result and Discussion

Figure 4.1 shows the time-lapsed images of a bilayer LEC tested under a temperature of 330 K and a constant bias voltage of 25 V. The gap size between the electrodes is 2 mm. The SPE underlayer has a KOTf: PEO weight ratio of 0.2. MEH-PPV was used as the conjugated polymer.

Figure 4.1(a) shows the photoluminescence (PL) under the illumination of a 365nm UV ring light. The MEH-PPV CP layer emitted uniform orange-red colored PL between the interelectrode gap. After applying the bias voltage, dark electrochemical p-doping started to grow from the anode due to heavy PL quenching. Meanwhile, faint electrochemical n-doping started to become visible on the cathode side. The p-doped and n-doped regions started to propagate toward each other at a constant speed until the furthest tips made contact and formed a local p-n junction after 15 seconds, as shown in Figure 4.1(c). The p-doping and n-doping propagation came to a stop once the doping fronts met each other and formed a p-n junction where electroluminescence (EL) was observed. As PL quenching and EL started to become stronger, a continuous light-emitting p-n junction has become visible as shown in Figure 4.1(e). Then, the continuous line of EL began to shift toward the cathode and became straightened out until it reached peak current at about  $t = 180$  s, as shown in Figure 4.1(g). The light-emitting p-n junction stayed in front of the p doping front throughout the entire shifting process. After 180 s, the brightness of the junction started to decrease, and the junction gradually stopped shifting as the cell current decreased.

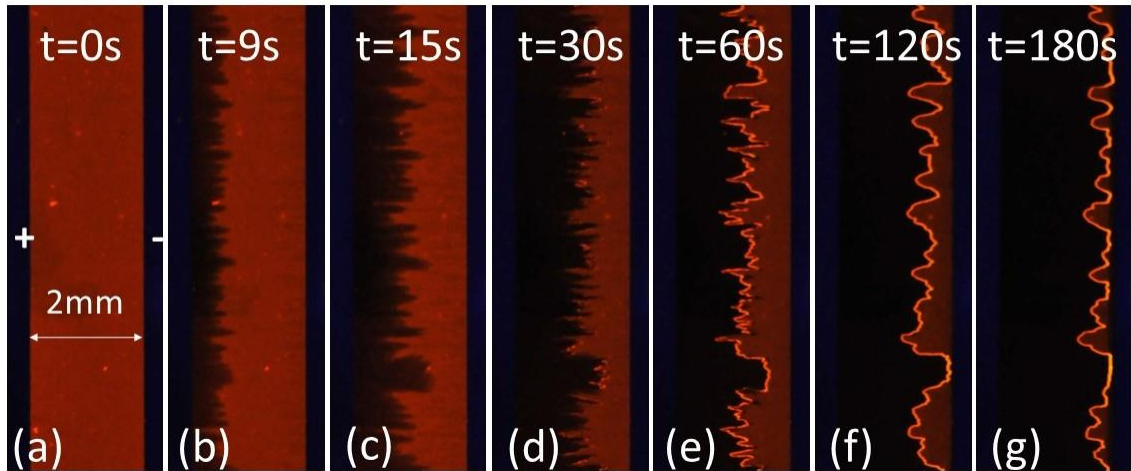


**Figure 4.1** A MEH-PPV/PEO:KOTf bilayer LEC tested under a constant bias voltage of 25V and a constant temperature of 330K. The images were captured under the illumination of a 365nm UV ring light from above.

Similar experiments were repeated for bilayer LECs with KOTf: PEO weight ratio of 0.4, 0.13, 0.1, 0.04, 0.025, 0.0125. Doping propagation and junction formation were observed in all devices, however, the difference in salt concentration led to a dramatic effect on cell current, doping propagation speed, and junction formation.

Figure 4.2 shows the current vs. time characteristics for bilayer LECs with different salt concentrations tested under a constant bias voltage of 25V and a constant temperature of 330K. All cells had an SPE layer thickness of  $400 \pm 40$  nm and MEH-PPV layer thickness of  $125 \pm 25$  nm. The same general trend was observed for devices with different salt concentrations.

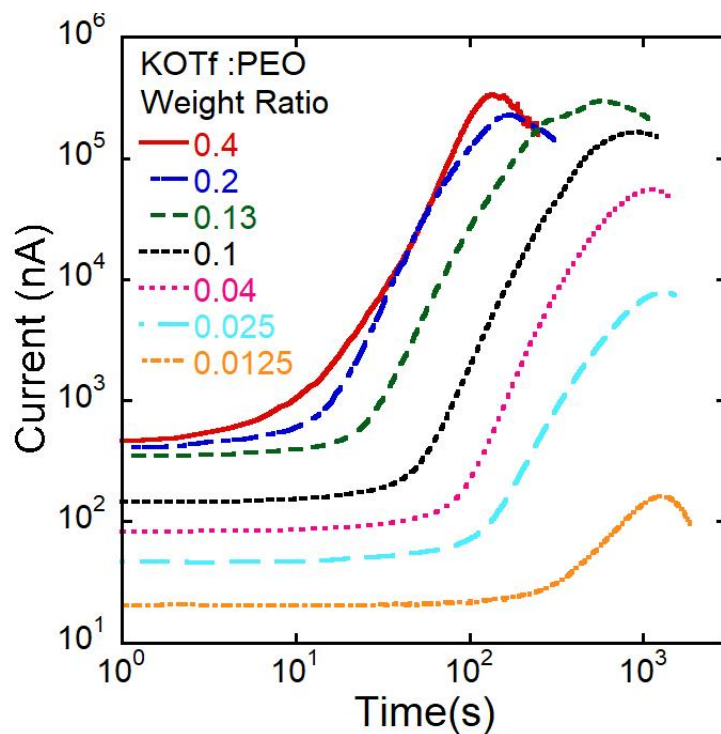


**Figure 4.2 Cell Current as a function of time for LEC devices with different salt concentrations tested under a constant bias voltage of 25V and a constant temperature of 330K.**

Shortly after applying a constant bias voltage to the cells, the cell current increased gradually as p-doped and n-doped regions began to grow. The initial cell current is strongly dependent on the salt concentration as shown in red squares in Figure 4.3. Since the cells were tested under a constant bias voltage, the increase in current suggested that there was a rise in cell conductance. A sharp rise in cell current was observed when p-doping and n-doping fronts made contact and formed a p-n junction, at which point, the time was determined as the initial junction formation time as shown in Appendix A and plotted in red dots in Figure 4.4. Upon the formation of a continuous light-emitting junction, the current exhibited a rapid growth until it reached the peak current. For most

cells, the cell current increased by at least two orders of magnitude as shown in Figure 4.3. Both initial current and peak current display a similar trend. The currents are linearly proportional to the salt concentration except for the highest salt concentration of 0.4. The cell with a salt concentration of 0.2 had an initial current of 407nA which is 20 times higher compared to the cell with a salt concentration of 0.0125. This initial current ratio is similar to the salt concentration ratio between the cells.

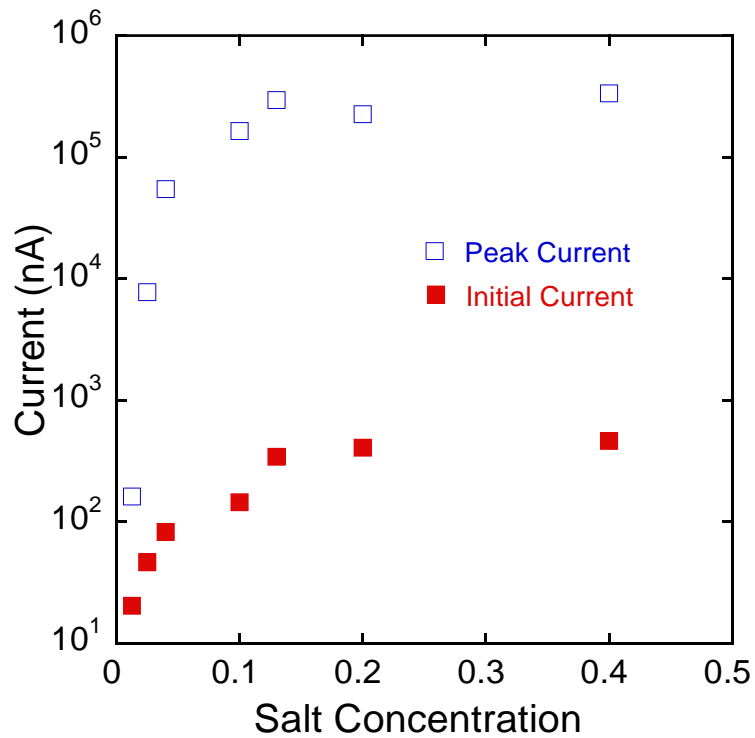


**Figure 4.3 Initial and peak current as a function of salt concentration under a constant bias voltage of 25V and a constant temperature of 330K.**

The increase in cell current suggested that conductivity of SPE is higher for devices with higher salt concentration. The conductivity  $\sigma$  can be presented as:

$$\sigma = n\mu e$$

where  $n$  is the number of ions, and  $\mu$  is the mobility of ions. The increase in salt concentration led to an increase in the number of ions which result in a higher conductivity. However, at high salt concentration, the increase in salt concentration led to a decrease in mobility, which explained the current leveling off at salt concentration of 0.4.

Alternatively, the initial junction formation times were determined by visually inspecting the time-lapsed images, as shown in Appendix A. The values of the two methods generally agree, that is, they fall within their respective range of uncertainties. The junction formation time was found inversely proportional to the salt concentration.

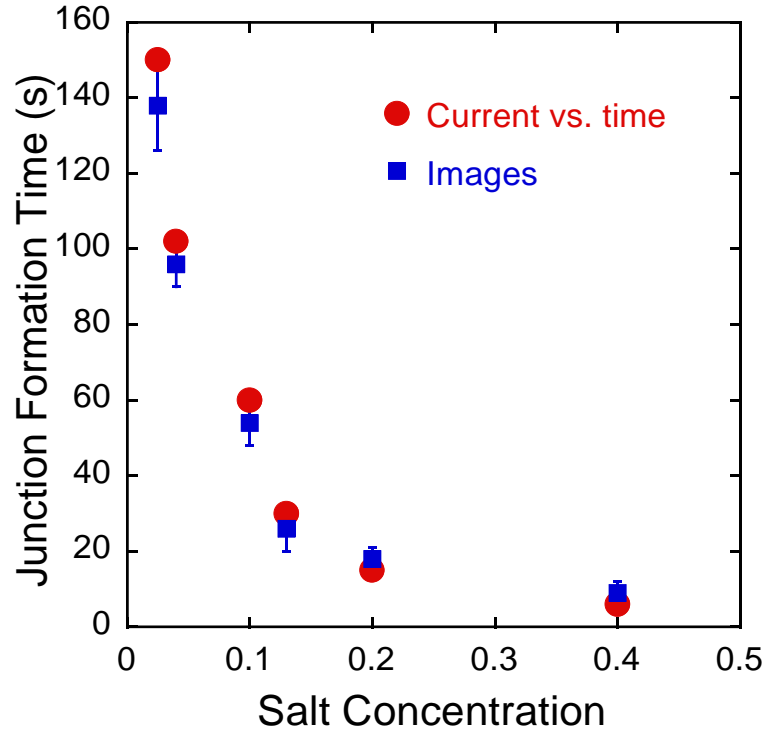


**Figure 4.4 Junction formation time as a function of salt concentration. The junction formation time was determined from current vs. time characteristics and the time-lapsed images and presented in red and blue, respectively. The methods for determining the junction formation times were described in Appendix A.**

Before the initial junction formation, the p-doping fronts moved toward the cathode at a constant speed. The average p-doping positions from the anode were extracted from the time-lapse images and plotted as a function of time in Figure 4.5. For all cells, the initial junction formation positions were approximately 1mm from the anode, that is, at the center of the 2mm interelectrode gap. However, there is one exception, which is the cell with a salt concentration of 0.025. The average initial junction position was 0.9mm from the anode caused by a jagged doping front.

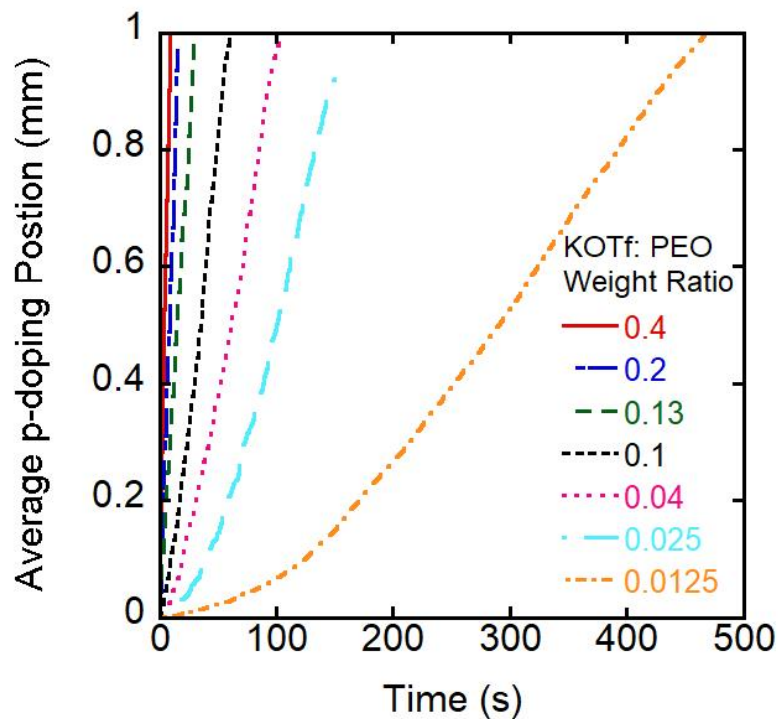


**Figure 4.5 Average p-doping position from anode as a function of time determined from the time-lapsed images.**

Except for the cell with the lowest salt concentration, which did not have a visible light-emitting p-n junction, the average p-doping position grew linearly with time. p-doping speed before junction formation was determined as the slope of the average p-doping position vs. time plot as shown in Figure 4.6. The salt concentration and the p-doping speed have a significantly positive correlation.

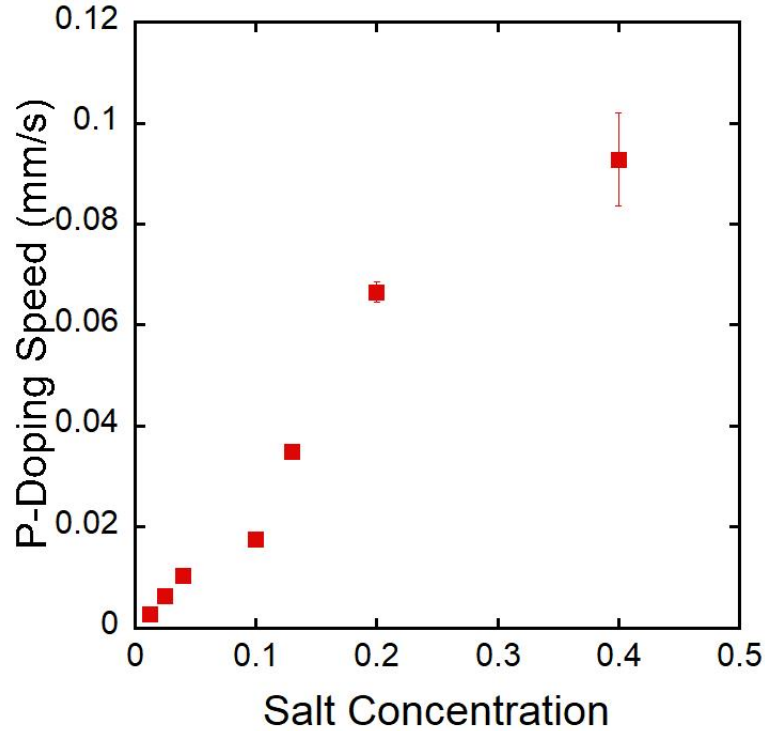


**Figure 4.6 p-doping propagation speed as a function of salt concentration. The average p-doping speed was determined as described in Appendix B.**

Attempts to turn on devices with a low salt concentration of 0.0125 was unsuccessful. Initially, the p-doping front grew slowly toward the cathode at a rate of 0.0027 mm/s, which is the slowest among all cells. At  $t = 360$ s, a sharp rise in current is observed, which suggested a p-n junction could have formed. However, there was no visible EL captured by the camera.

Upon the formation of a continuous light-emitting junction, the junction position began to shift toward the cathode side until the current reached the maximum. After the current reached the peak value, the junction position gradually stopped shifting, and the light-emitting junction began to fade as the current decreased. However, the shift of the junction position is not consistent for cells with different salt concentrations. The images

captured at peak current for LECs with different salt concentrations are shown in Figure 4.7(a)-(f). For the cell with the highest salt concentration of 0.4, the continuous EL junction shifted away from the anode aggressively until it reached the cathode. However, for the cell with the lowest salt concentration of 0.025, there was barely any shift in the junction position. The EL zone was about 1 mm from the anode which was similar to the initial junction formation position. The average junction positions relative to the anode were calculated and plotted in Figure 4.7(g). The junction position at peak current is proportional to the salt concentration. Since an EL zone away from the metal electrode is preferred in LECs due to the latter's luminescence quenching effect, this effect has the potential to be utilized to optimize cell performance.

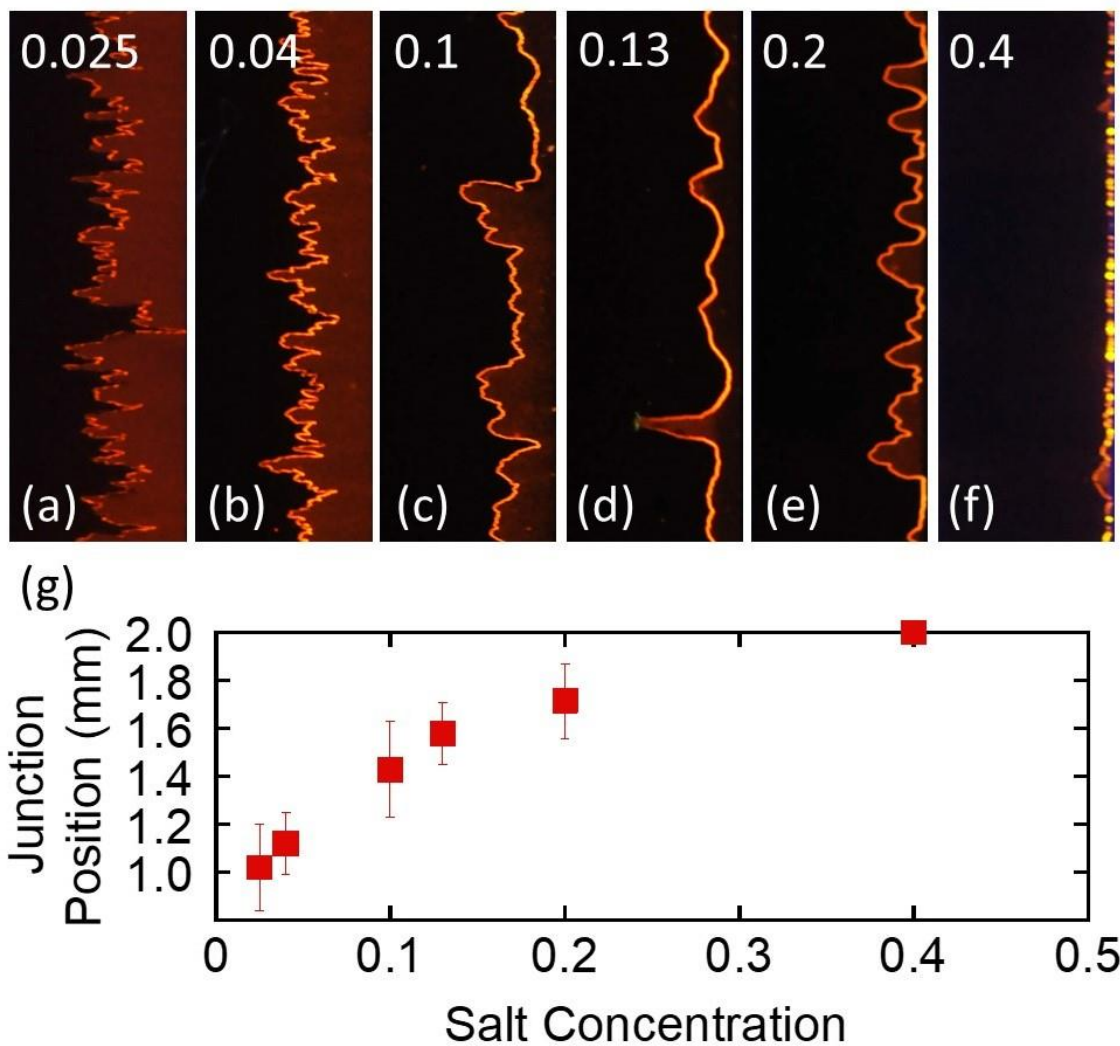


**Figure 4.7 (a)-(f) Images taken at peak current for LECs with different salt concentrations. (g) Average junction position relative to the anode as a function of salt concentration.**

Figure 4.8 shows the DC cell resistances between the electrodes after doping was initiated but before junction formation. The doped CP is highly conductive as mobile ions are injected and play a role of counter ions. p-doped and n-doped regions are making contact with both undoped CP and the SPE underlayer, which forms a parallel circuit. This model is simplified under the assumption that other resistance, such as contact resistance between the electrode and doped CP, ionic resistance from electrode migration, and interfacial resistance between the CP layer and the SPE layer; are ignored as they are not limiting resistance. [41] Since undoped CP has negligible conductance, the cell current is directly limited by the resistance of the SPE layer. This explains the linear dependence between the cell current and the salt concentration under a constant bias voltage. The linear relationship between current and salt concentration suggested that the ion mobility is not affected by the salt concentration if the salt concentration is below 0.2. However, at high salt concentrations, the formation of ionic bond pairs led to a decrease in ionic conductivity, which explains the current leveling off at high salt concentrations of 0.2 and 0.4. [42] This behavior was proven by the experimental measurements of the ionic conductivity of the PEO electrolyte. [43][44]

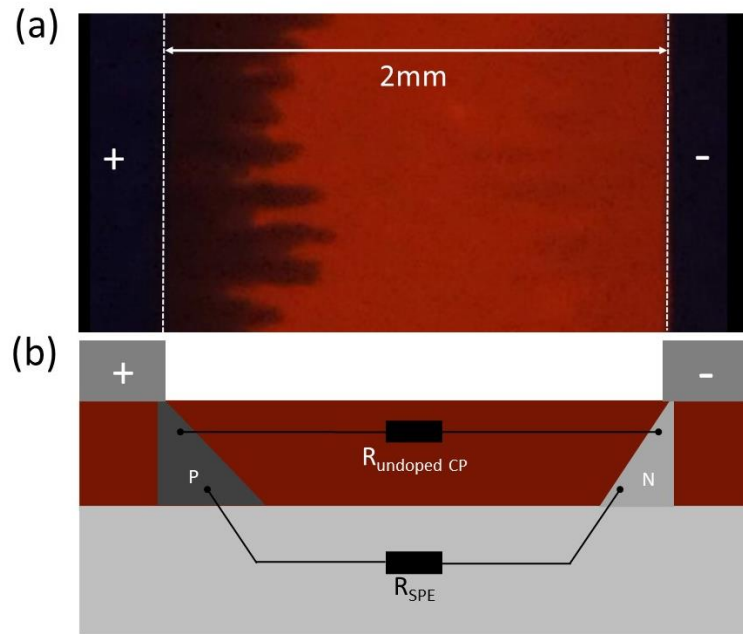


**Figure 4.8 (a) PL image showing a typical doping profile before junction formation. (b) A schematic showing the cross-section of bilayer cell before junction formation.**

### 4.3 Conclusion

In this chapter, the effects of salt concentration have been visualized in bilayer planar LECs with a gap size of 2mm. Electrochemical doping and light-emitting EL junction was observed for all devices with a salt concentration higher than 0.025 under a constant bias voltage of 25V and a constant temperature of 330K. The cell current, doping propagation speed, and junction formation time were strongly dependent on the salt concentration in the SPE. This suggested that the performance of LECs is limited by the resistance of the SPE. Moreover, the junction position was found to change with the salt concentration. This behavior has the potential to improve the performance of LECs by modifying/controlling the position of the EL junction.

## Chapter 5

### Effects of SPE Layer Thickness

#### 5.1 Introduction

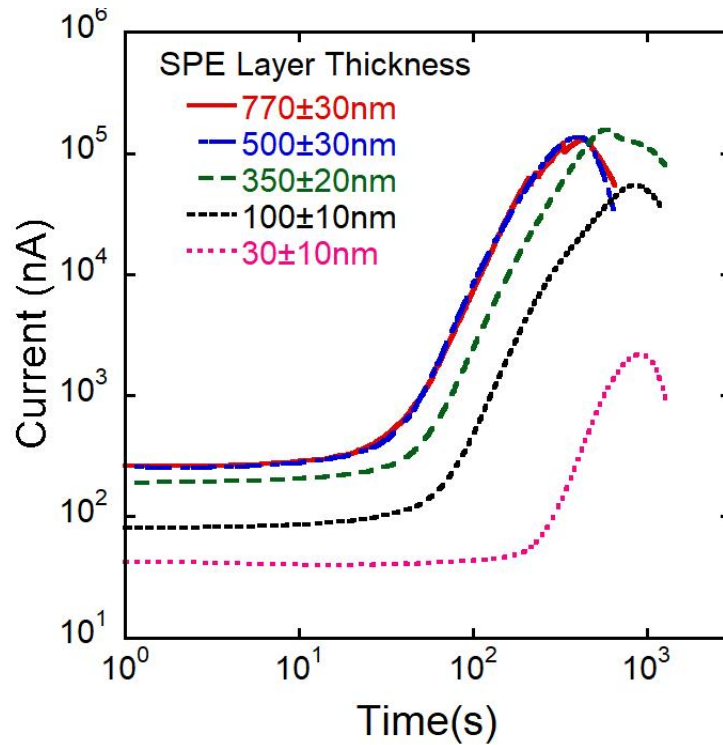
In the previous chapter, the effects of salt concentration were visualized in bilayer planar LECs. The results provided direct evidence that the performance of LECs is limited by the ionic resistance of the SPE layer. In addition to salt concentration, the ionic resistance of the SPE layer can also be limited by the thickness. The thickness of the SPE layer was modified by diluting the PEO: KOTf solution and varying the initial spin speed when casting the thin polymer layer as shown in Table 5.1. Bilayer cells with SPE layer thickness ranging from  $770 \pm 30\text{nm}$  to  $30 \pm 10 \text{ nm}$  will be presented and discussed in this chapter. All devices have a 0.13 PEO/KOTf weight ratio in the SPE layer.

Initial Spin Speed (RPM)	Dilution Factor	SPE layer Thickness (nm)
1000	1	$770 \pm 30$
2000	1	$500 \pm 30$
4000	1	$350 \pm 20$
4000	2	$100 \pm 10$
4000	3	$30 \pm 10$

**Table 5.1 Thickness of SPE layer by varying initial spin speed and solution dilution factor.**

## 5.2 Result and Discussion

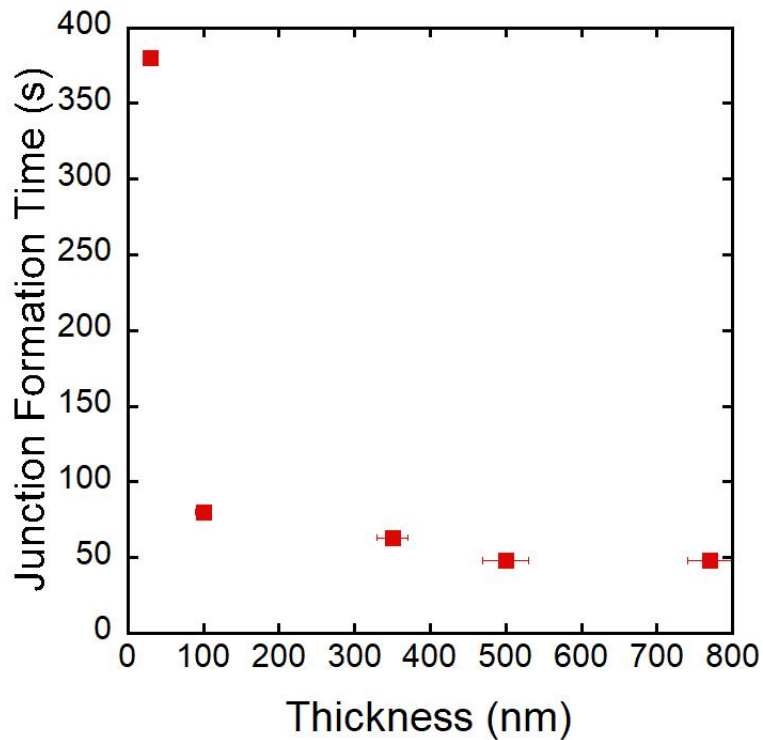
Figure 5.1 shows the cell current as a function of time for LEC devices with different SPE layer thicknesses. All devices are tested under a constant bias voltage of 15V and a constant temperature of 330K. The current vs time curves exhibit the same shape and general trend similar to observations in Chapter 4.



**Figure 5.1 Cell Current as a function of time for LEC devices with different SPE layer thickness tested under a constant bias voltage of 15V and a constant temperature of 330K.**

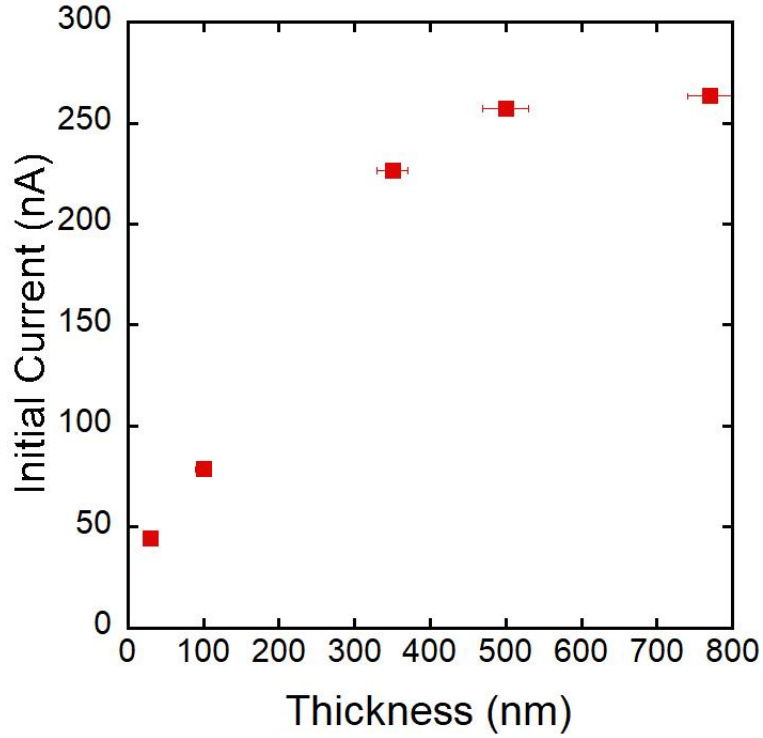
The cell current for devices with SPE layer thickness of 770 nm and 500 nm are identical, suggesting that ions more than 500nm away from the CP layer did not contribute to the doping reaction. The initial junction formation time was extracted by fitting the current vs time curve in the logarithmic scale, presented in Figure 5.2. Except for the device with

the thickest SPE layer, the initial junction formation time is inversely proportional to the thickness of the SPE layer.



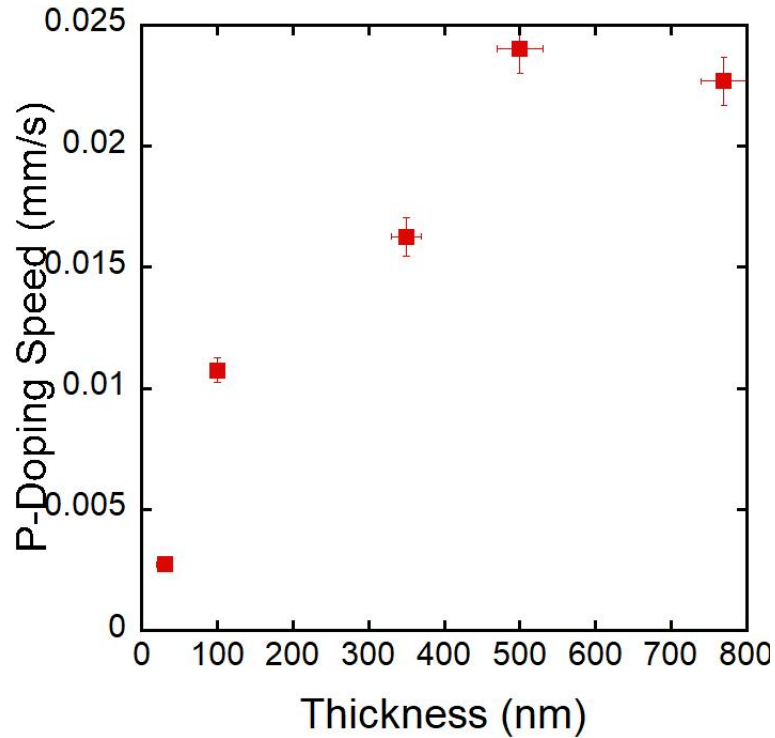
**Figure 5.2 Junction formation time as a function of SPE layer thickness. The junction formation times were determined from the current vs. time curves as described in Appendix A.**

Figure 5.3 shows the initial current as a function of SPE layer thickness. For cells with a thinner SPE layer, the initial current was found linearly proportional to the thickness, while a current leveling off was observed when the thickness of the SPE layer reached more than 500 nm.



**Figure 5.3 Initial cell current as a function of SPE layer thickness.**

The position of the p-doping fronts was extracted from the time-lapse images and the average p-doping speed was determined and presented in Figure 5.4. For devices with a thinner SPE layer, p-doping fronts moved at a constant speed uniformly toward the cathode. As the thickness of the SPE layer increases, the cell surface became less uniform, which leads to more jagged p-doping and n-doping fronts.



**Figure 5.4 Average p-doping speed as a function of SPE layer thickness. The average p-doping speed was determined as described in Appendix B.**

Figure 5.5 shows the time-lapsed images captured at the same time for cells with SPE layer thicknesses of 770 nm and 500 nm. The average doping front position was found similar at the same time. As the SPE layer went beyond 500 nm in thickness, there were no improvements in cell current and doping propagation speed, however, the doping fronts were more jagged due to a less uniform polymer film surface.

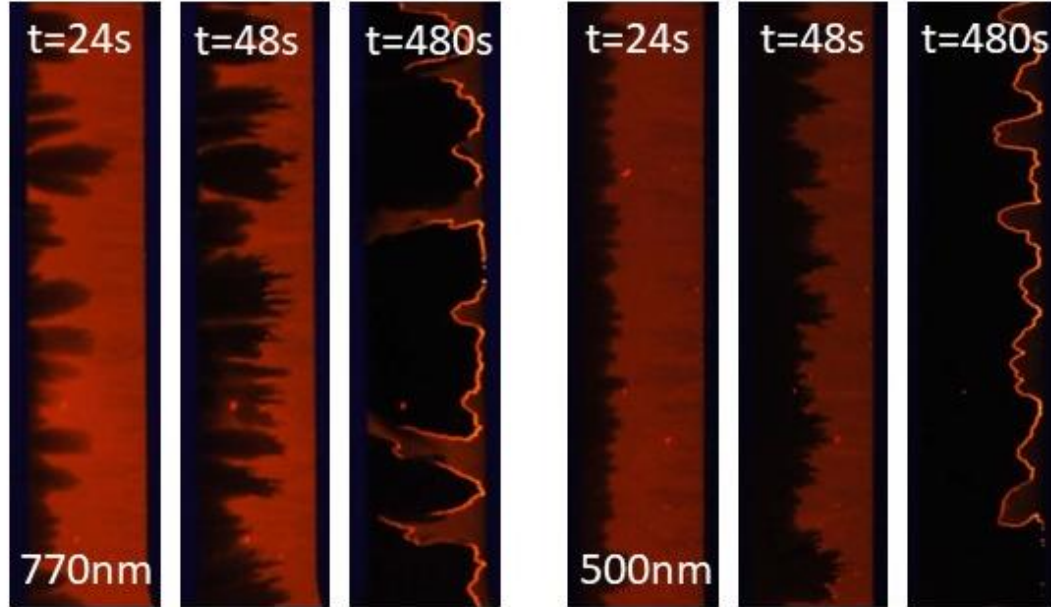


**Figure 5.5 Time-lapsed images captured for bilayer LECs with SPE layer thickness of 770 nm and 500 nm.**

### 5.3 Conclusion

In this chapter, the effects of SPE layer thickness have been visualized in bilayer planar LECs with a gap size of 2 mm. Electrochemical doping and light-emitting EL junction was observed for all devices with an SPE layer thickness between 770 nm and 30 nm tested under a constant bias voltage of 15 V and a constant temperature of 330 K. A SPE layer thinner than 500 nm led to a decrease in cell current and doping propagation speed. The position of the p-n junction is not thickness dependent. The results suggested that the conductance of the cells is proportional to the thickness of the SPE, which further proved that the LEC performance is limited by the resistance of the SPE layer.

## Chapter 6

### Effects of Cation

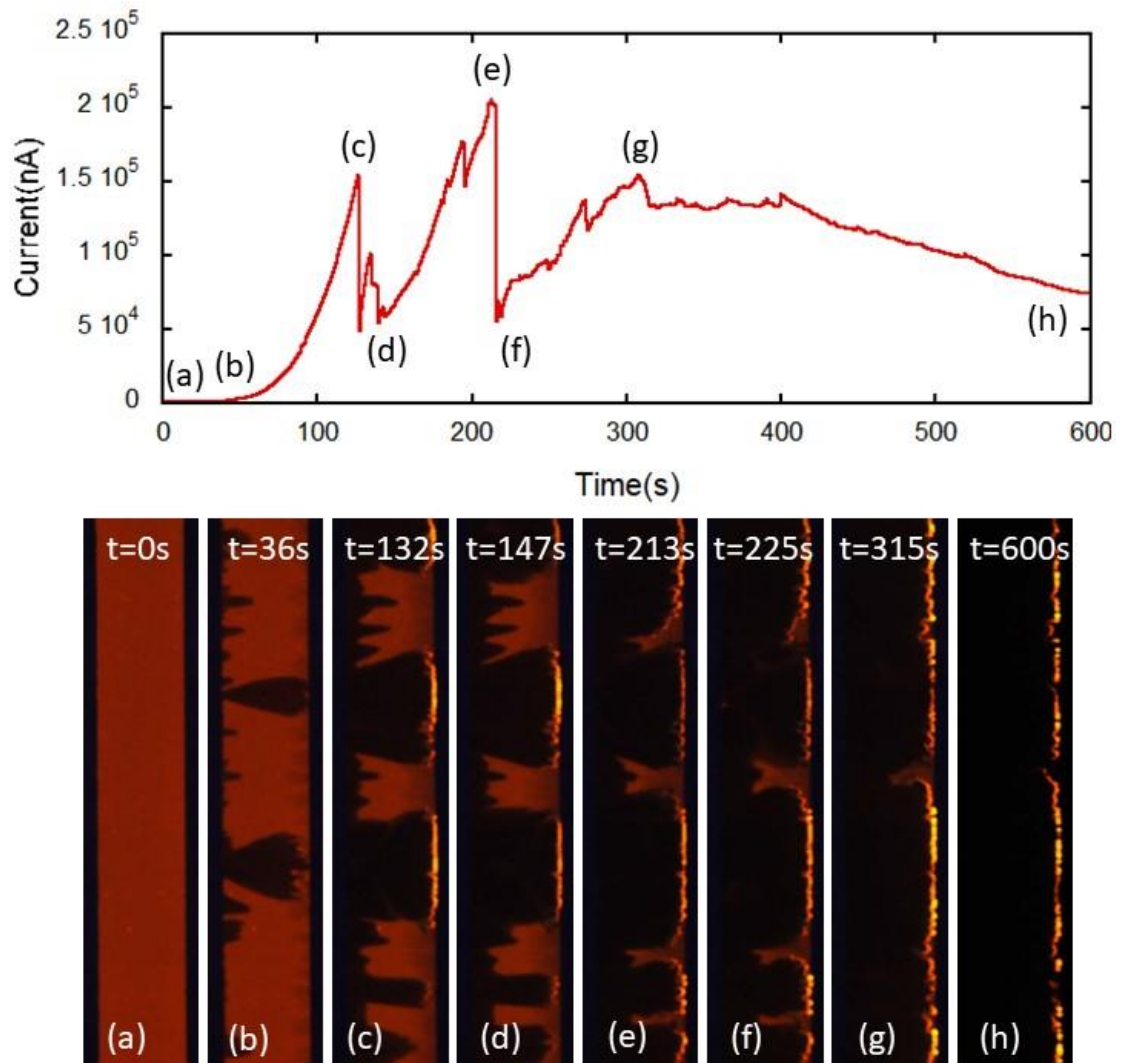
#### 6.1 Introduction

The results in Chapter 4 and Chapter 5 provided direct evidence that the performance of LECs was limited by the resistance of the SPE. The difference in conductance was achieved by modifying the amount of ions in the SPE under the assumption that the ionic mobility is not affected by the salt concentration or the thickness of the film. The conductivity of SPE is also strongly dependent on the size and mass of cations. [45] An early study on single layer planar LECs found that the speed of doping propagation and the position of the light emitting p-n junction were both strongly dependent on the size of salt cations. [46] In bilayer planar LECs, the ion transport is not affected by the presence of CPs. Similar or stronger cation effects on doping propagation is expected. In this chapter, bilayer LECs with different cations are demonstrated and discussed.

## 6.2 Result and Discussion

### 6.2.1 Alkali Metals

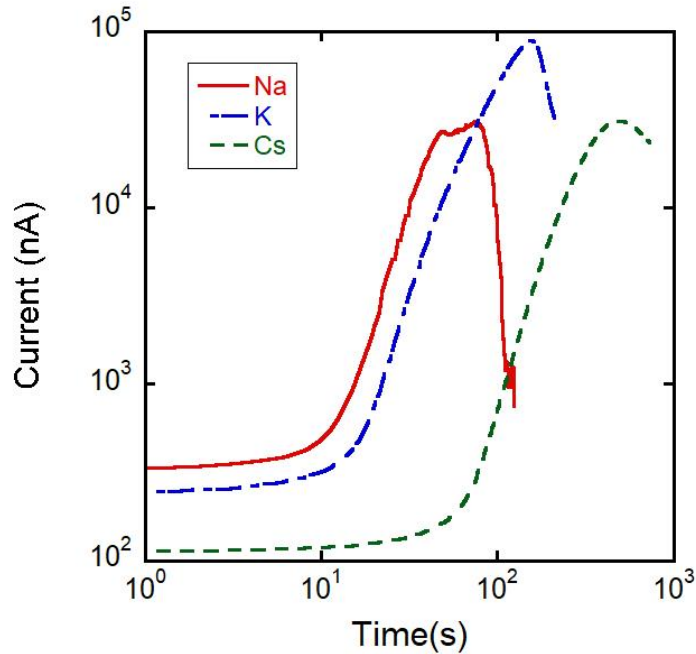
Figure 6.1 shows the current vs. time characteristics of bilayer LEC with a Li salt. Unlike other LEC devices, the current experienced three peaks when tested under a constant bias voltage. Immediately after applying a constant bias voltage of 25V, dark p-doping fronts started to propagate from the anode while faint n-doping was observed from the cathode. The furthest tips of p-doped and n-doped regions made contact after 36 seconds and formed an isolated light emitting p-n junction as shown in Figure 6.1(b). However, a sharp rise in current was not observed until 52 seconds. As the p-doped and n-doped regions grew in size, the current reached the first peak at  $t=132s$ , where three discontinuous local light emitting p-n junctions were observed as shown in Figure 6.1(c). Then, the cell current experienced a sudden drop until 147 seconds. As shown in Figure 6.1(d), the position of the p-doping and n-doping front remained the same during the current drop. As the p-doped region started to propagate and merge, the cell current reached the maximum at  $t=213s$ , from where a sharp drop in current was observed. Similarly, the position of doping fronts and the p-n junction did not move as shown in Figure 6.1(e)-(f). As most of the interelectrode region was doped and became dark due to heavy PL quenching, the cell current reached its third peak after 315 seconds. A continuous light-emitting p-n junction was observed right next to the cathode. The junction EL started to fade as the cell current gradually decreased.



**Figure 6.1** Current vs time characteristics for MEH-PPV/PEO/LiClO<sub>4</sub> bilayer LEC tested under a constant bias voltage of 25V and a constant temperature of 330K. (a)-(h) Time lapsed images captured under the illumination of a 365nm UV ring light from above.

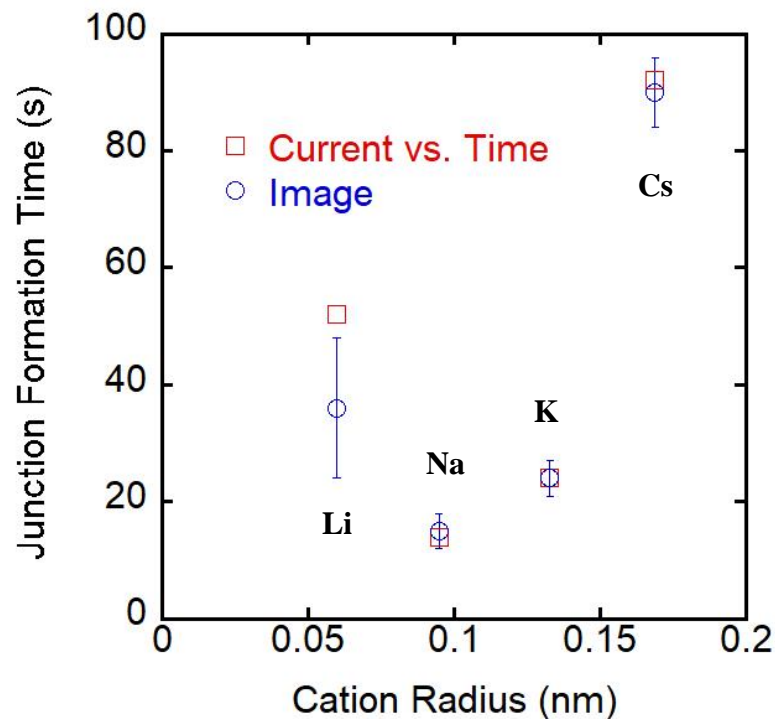
Similar tests were performed for LEC devices with three other alkali metal cations; Na, K, and Cs. (Note that Rb device was not tested due to poor solubility in cyclohexanone and PEO).

Figure 6.2 shows the current vs. time characteristics for bilayer LEC devices with different alkali metal cations. Similar to other bilayer LECs devices, the same general trend was observed.



**Figure 6.2 Cell Current as a function of time for LEC devices with different alkali metal cations tested under a constant bias voltage of 25V and a constant temperature of 330K.**

The current experienced a sharp rise when the furthest tip of n-doped and p-doped regions made contact and formed local light emitting p-n junction. The initial junction formation times were analyzed by fitting the curve on logarithm scale and presented in Figure 6.3 as red squares. The initial junction formation time was also determined by visualizing the time-lapsed images and presented in Figure 6.3 as blue circles. The values of the two methods fall within their respective range of uncertainties except for the cells with the Li salt device.



**Figure 6.3 Junction formation time as a function of cation radius. The junction formation time was determined from current vs. time characteristics and the time-lapsed images and presented in red and blue, respectively. The methods for determining the junction formation times were described in Appendix A.**

The initial cell current is affected by the size of the cations as shown in Figure 6.4. The initial cell current was found to be inversely proportional to the cation radius, which suggests that the increase in cation size result in a drop in cell conductance.

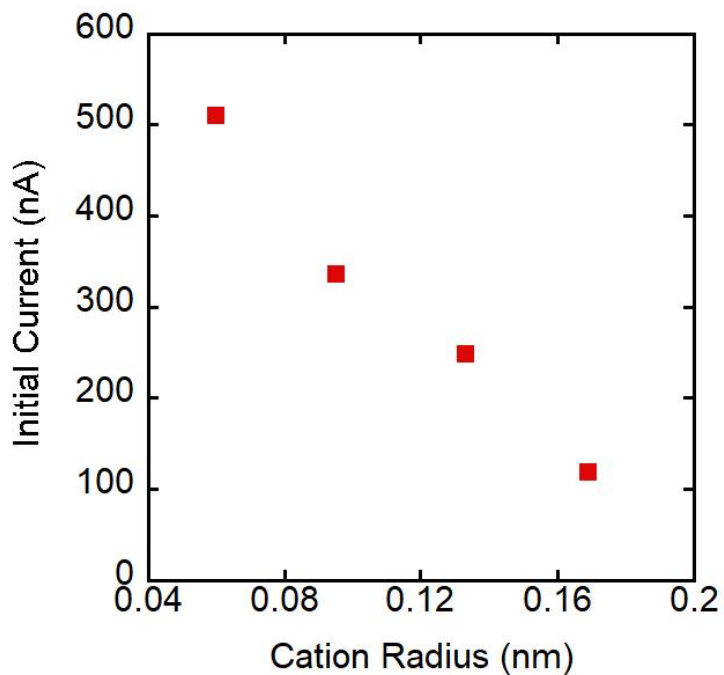


**Figure 6.4 Initial current as a function of cation radius under a constant bias voltage of 25V and a constant temperature of 330K.**

Similar to the observation of single layer devices with different cations, the junction position at peak current was found dependent on the size of the cations. The images capture at peak current under the illumination of a 365nm UV ring light from above for cells with different cations are shown in Figure 6.5.

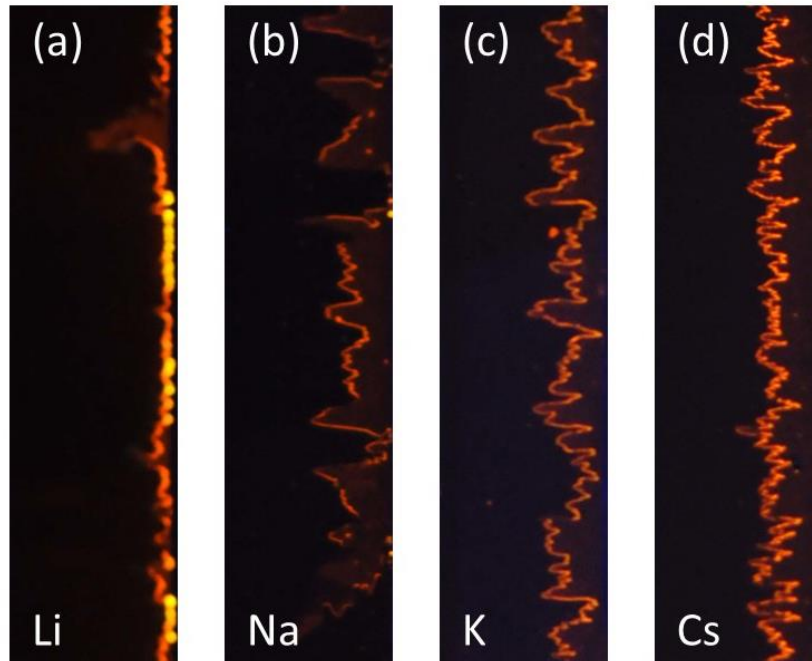


**Figure 6.5 Images captured at peak current for LECs devices with (a) Li salt (b) Na salt (c) K salt (d) Cs salt**

Figure 6.6 shows the average normalized junction position at peak current as a function of cation radius for alkali metals. Note that single-layer devices have an interelectrode gap size of 11mm retrieved from [46]. Bilayer devices have an interelectrode gap size of 2mm. The junction position was extracted by visually investigating the images captured at peak current. Normalized junction position was calculated as the ratio between junction position and interelectrode gap size. For both configurations, the junction position was closer to the anode with increasing cation size.

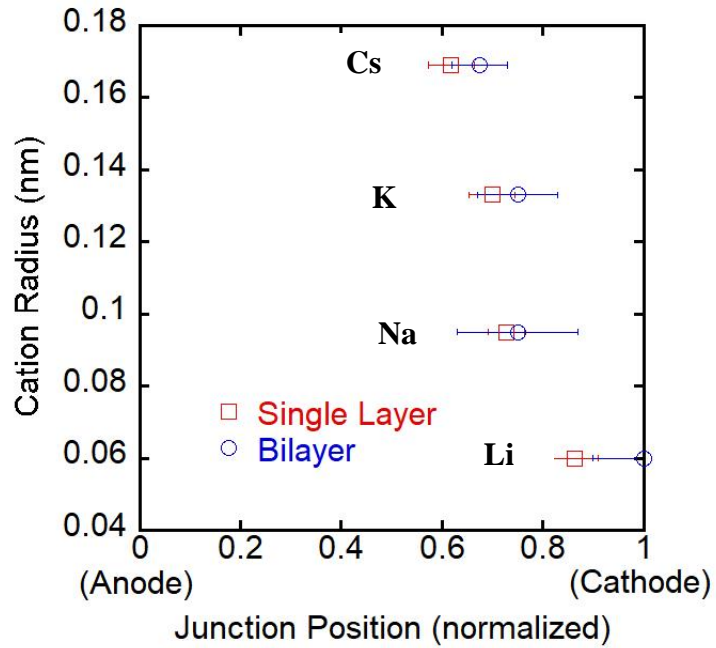


**Figure 6.6** The normalized junction position at peak current (relative to anode) as a function of cation radius. Bilayer data were extracted from the time-lapsed images of devices with 2mm gap size. Single layer data were taken from devices with gap size of 11mm. [46]

### 6.2.2 Transition Metals

In addition to salts with alkali metals cations, LEC devices with transition metal cations trifluoromethanesulfonate salts; zinc trifluoromethanesulfonate (ZnOTf), europium trifluoromethanesulfonate (EuOTf), terbium trifluoromethanesulfonate (TbOTf); were tested under the same test conditions, which is a constant bias voltage of 25V and a constant temperature of 330K. However, there was no doping or any increase in the cell current observed. The cell with Zn salt only had an initial current of 9.1nA, whereas the initial current for the cell with Tb salt was approximately zero. The cell currents were more than two orders in magnitude smaller compared to the cells with alkali metal cations, which suggested that the increase in cation size reduced the conductance of the cells, which limited the cell current and the initialization of the doping process.

Higher bias voltage and temperature were applied to turn on cells with larger cation sizes. Figure 6.7 shows the time-lapsed images captured for the bilayer LEC device with ZnOTf salt tested under a constant bias voltage of 100V and a constant temperature of 360K. Immediately after applying a constant bias voltage, dark p-doping was observed from the anode as shown in Figure 6.7b. The p-doped fingers started to propagate toward the cathode as well as in a direction parallel to the electrodes, which forms a balloon-shaped p-doped region as shown in Figure 6.7c. During the propagation of the p-doped region, n-doping was not observed from the cathode. As the furthest tip of the p-doped regions reached the cathode, local light emitting p-n junction was formed next to the cathode as shown in Figure 6.7d. As the p-doped region continued to grow, red-orange colored PL started to fade due to PL quenching, and a continuous light emitting p-n junction was observed at about  $t=60s$  as shown in Figure 6.7f. The intensity of EL became stronger as

the cell current continued to increase until it reached its peak. There was no shift in the junction position after initial junction formation.

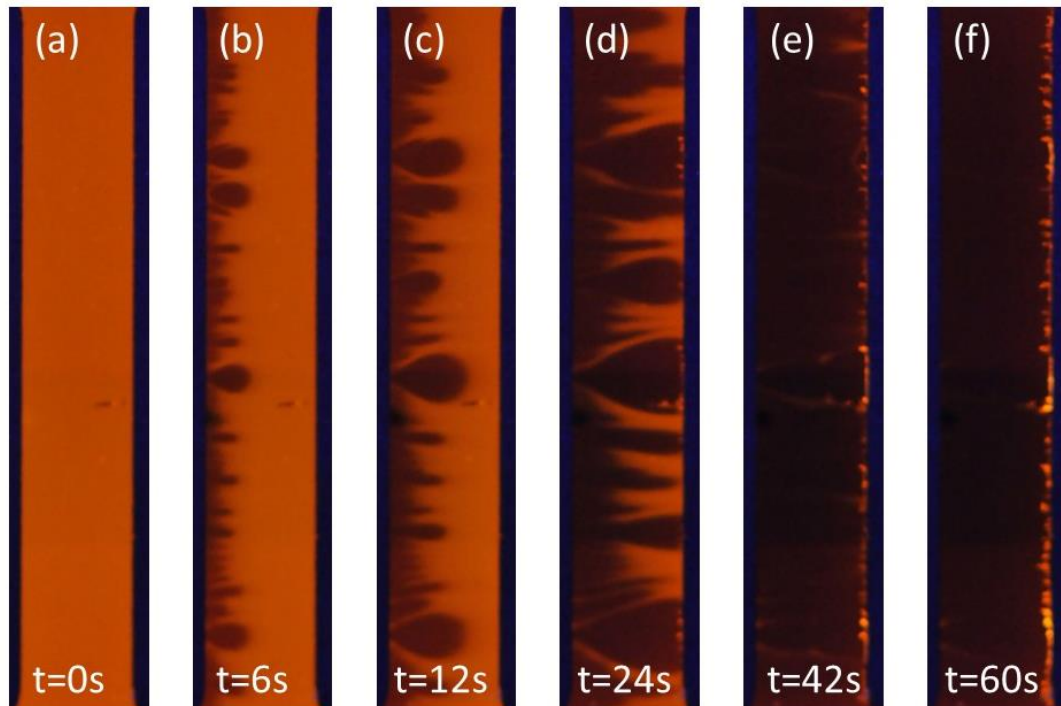


**Figure 6.7 Time-Lapsed images for bilayer LEC device with ZnOTf salt tested under a constant bias voltage of 100V and a constant temperature of 360K.**

Cells with Eu salt were tested under a constant bias voltage of 100V and a constant temperature of 360K, the time-lapsed images are shown in Figure 6.8. Dark p-doping was observed from the anode, however, there was no visible n-doping. As the cell current increased linearly, the p-doped region propagated towards the cathode until made contact. The PL between electrodes disappeared due to heavy PL quenching. There was no visible light-emitting p-n junction as the p-doped region made contact with the cathode. To turn on the device with Eu salt, the same device was tested under a constant bias voltage of 200V. By doubling the bias voltage, a sharp rise in current was observed when

a local light emitting p-n junction was formed. As the p-doped region continued to propagate toward the cathode, a continuous EL junction was formed next to the cathode.

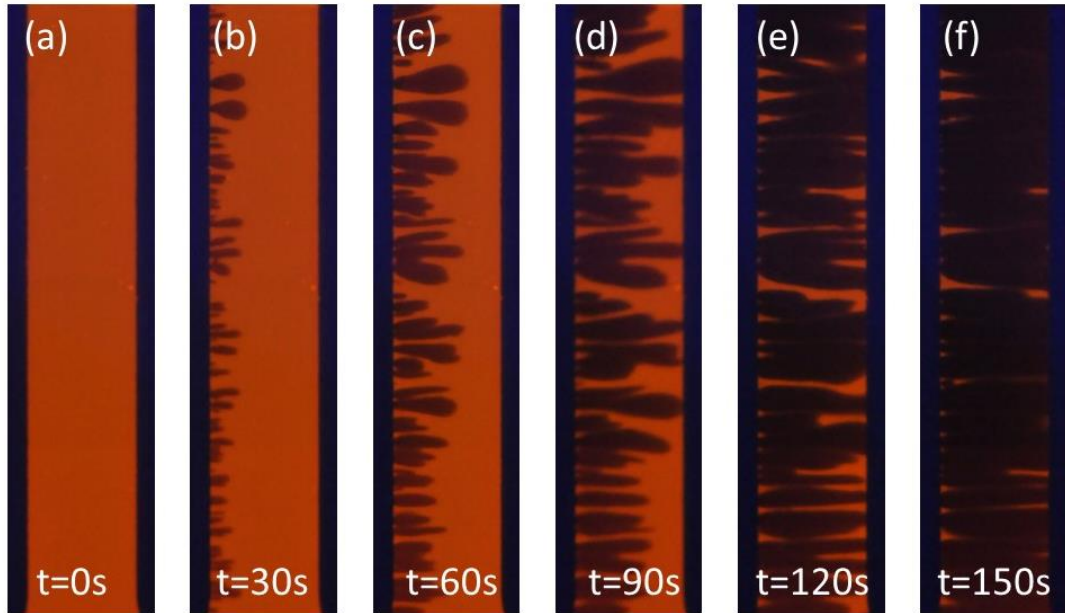


**Figure 6.8 Time-Lapsed images for bilayer LEC device with EuOTf salt tested under a constant bias voltage of 100V and a constant temperature of 360K.**

Bilayer LECs with TbOTf salt were tested by increasing the bias voltage to 200V and the temperature to 360K. A slight increase in initial cell current was observed as the bias voltage was increased, however, there was no increase in current under constant bias voltage and no doping was observed.

### 6.2.3 Ammonium

To further explore the effect of cations, LECs devices with ammonium trifluoromethanesulfonate (AmOTf) salt were tested under a constant bias voltage of 25V and 330K. Figure 6.9 shows the time-lapsed images captured under a constant bias voltage of 25V and a constant temperature of 330K. Dark p-doping grew from the anode and propagated towards the cathode, while no n-doping was observed. A continuous light-emitting p-n junction was observed as the p-doped region made contact with the cathode as shown in Figure 6.9f. The position of the junction was next to the cathode and no shift in junction position was observed.

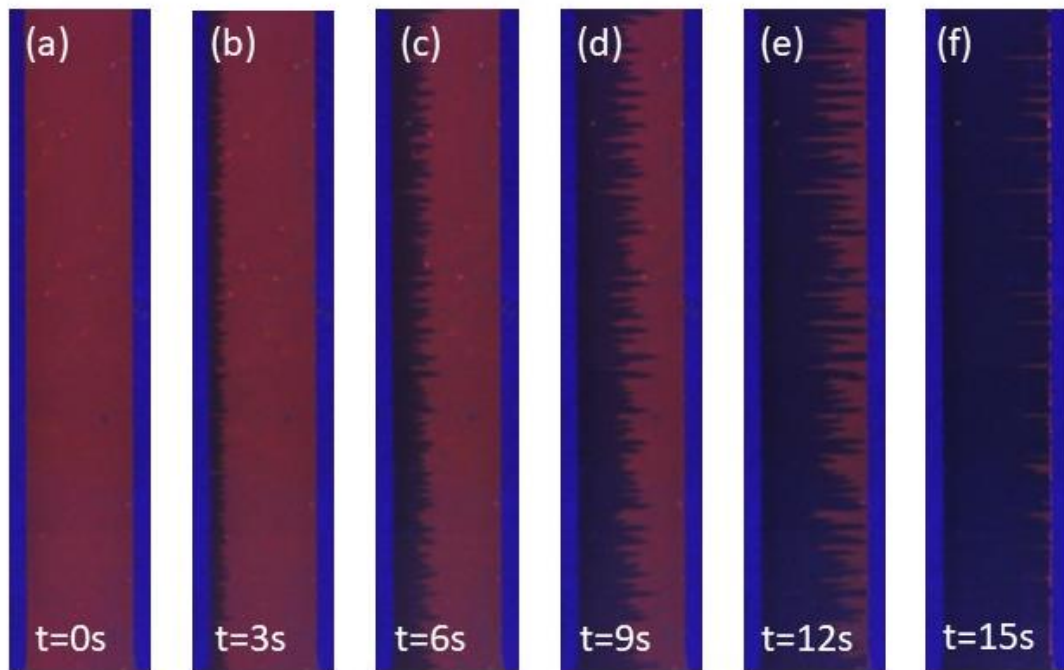


**Figure 6.9** Time-Lapsed images for bilayer LEC device with AmOTf salt tested under a constant bias voltage of 25V and a constant temperature of 330K.

A single layer LEC with the same composition of AmOTf was fabricated and tested under the same test conditions, which is a constant bias voltage of 25V and a constant temperature of 330K. Figure 6.10 shows the time-lapsed images captured for a single-layer device with AmOTf salt. Compared to bilayer devices tested under the same test condition, the general shape and size of the p-doped figures are similar, while for both configurations, n-doping was not observed. The doping propagation speed for single layer devices is slower compared to bilayer devices. For a single-layer device, it took three times longer for p-doping to reach the cathode, however, for EL was not observed as the p-doped region made contact with the cathode as shown in Figure 6.10e.

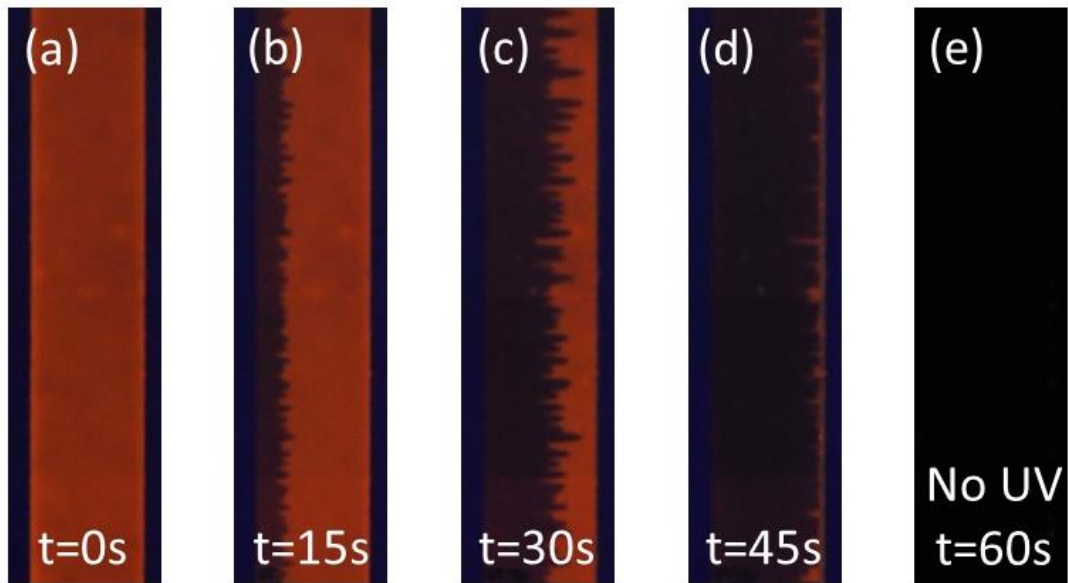


**Figure 6.10 Time-Lapsed images for single layer LEC device with AmOTf salt tested under a constant bias voltage of 25V and a constant temperature of 330K. (a)-(d) captured under the illumination of a 365nm UV ring light from above. (e) captured with no additional light source.**

The current vs. time characteristics for single layer and bilayer LEC devices with AmOTf salt under a constant bias voltage of 25V were presented in Figure 6.11. The single layer device had an initial current of 1785 nA which is twice as large compared to the bilayer device which had an initial current of 812 nA. For single-layer devices, the current kept decreasing under a constant bias voltage. The cell current of the bilayer device, however, experienced a sharp increase upon the formation of the p-n junction and reached a peak current of 20 times higher in magnitude. The outperformance of the bilayer device relative to the single layer device suggested that the ion insertion from the SPE to the CP was not the limiting factor of the poor current behavior in devices with large cation size, which further proves that the performance of LECs were limited by the resistivity of the SPE.

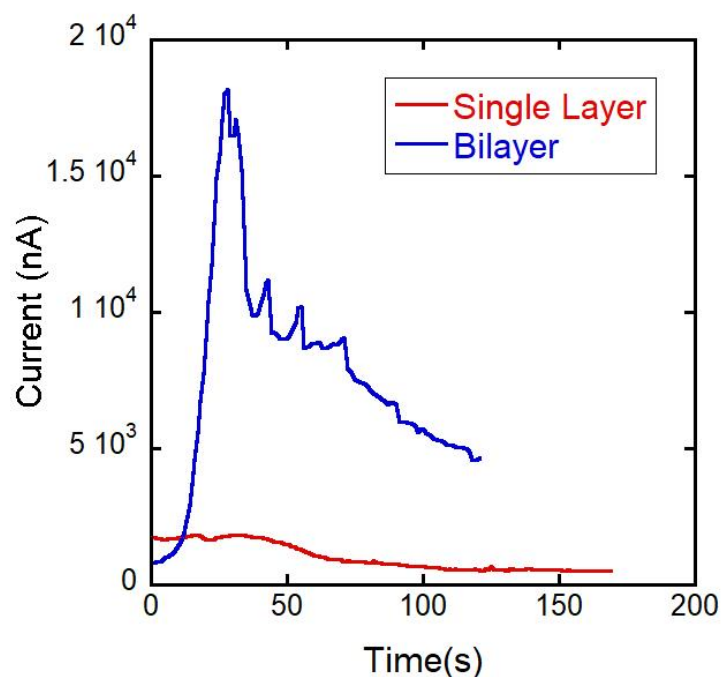


**Figure 6.11 Cell Current as a function of time for single layer and bilayer LEC devices with AmOTf salt tested under a constant bias voltage of 25V and a constant temperature of 330K.**

Ammonium cations and potassium cations are similar in size, however, LECs with ammonium and potassium salts had different current and doping behaviors under the same test conditions. Figure 6.12 shows the current vs time characteristics for bilayer LEC devices with ammonium and potassium salt tested under a constant bias voltage of 25V and a constant temperature of 330K. The initial current of the ammonium salt device was twice as large compared of the potassium salt device; however, the peak current of the potassium salt device was more than one order higher in magnitude. The initial junction formation time was similar (~12s for ammonium, ~15s for potassium), however, the average p-doping speed for the ammonium salt device was about twice as fast because there was no n-doping observed for the ammonium device.

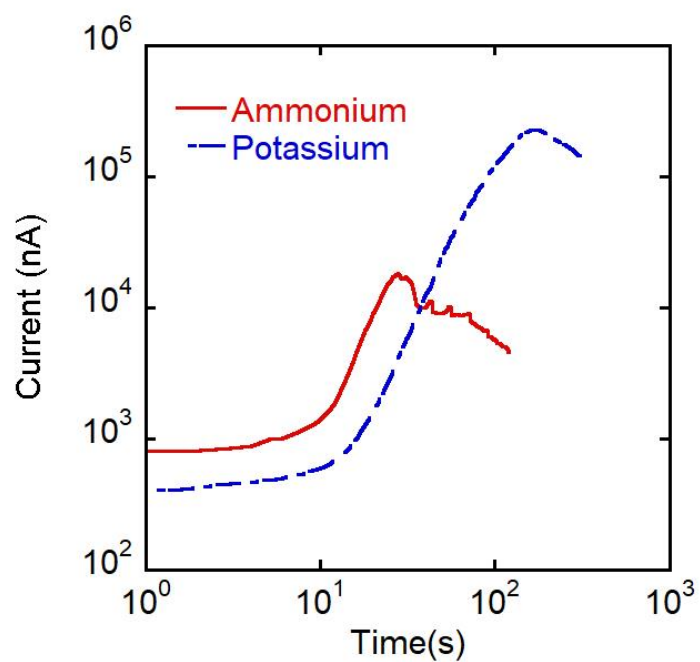


**Figure 6.12 Cell Current as a function of time for bilayer LEC devices with AmOTf and KOTf salt tested under a constant bias voltage of 25V and a constant temperature of 330K.**

### 6.3 Conclusion

In this chapter, the effects of the size and the mass of cations in the SPE layer of bilayer LECs were visualized and investigated. Devices with different cations were fabricated with the same ionic concentration and tested under a constant bias voltage and a constant temperature. For devices with alkali metal cations, the increase in the size and the mass of cations led to a decrease in the initial cell current. The positions of the junction at peak current were closer to the anode (more centered) as the size of the cations increased, which provided a similar trend compared to single layer devices. Except for cells with lithium cations, which behaved as an outlier due to jagged doping fronts, the increase in the cation size caused a slower doping speed and junction formation. Similar tests were performed on devices with larger transition metal cations. Doping propagation was not observed under the same test conditions because of the decrease in the conductivity due to large cation sizes. Devices with Zn and Eu cations were successfully turned on with higher bias voltage and temperature, however, the junction positions were next to the cathode, and no n-doping was observed. The attempts to turn on devices with Terbium cations were not successful. Lastly, devices with ammonium cations were fabricated and tested. Even though the size of ammonium cation is similar to potassium cation; cell current, doping propagation speed, and junction position showed a completely different behavior, which provided direct evidence that the size of the cations was not the only factor that affected the cell behaviors.

## Chapter 7

### Extremely Low Salt Concentration Devices

#### 7.1 Introduction

In Chapter 4, the effects of salt concentration on 2mm bilayer LECs were visualized and discussed. The decrease in salt concentration led to a decrease in cell current, doping propagation speed, and junction formation time. Under the test conditions of a constant bias voltage of 25V and a constant temperature of 330K, devices with a salt concentration of 0.0125 was not successfully turned on. However, a sharp rise in current was observed as p-doping and n-doping fronts met, which is strong evidence that the p-n junction was formed. Recent studies on bilayer LECs suggested that the cell current is strongly dependent on bias voltage and temperature [41], which made it possible to turn on bilayer devices with lower salt concentrations. For sandwich cells with silver salt, devices with salt concentration as low as 0.0005 was successfully turned on [47], however, for bilayer planar cells, the lower limit for salt concentration was never investigated. In this chapter, 2mm bilayer planar LECs with extremely low salt concentration will be visualized and discussed.

## 7.2 Result and Discussion

By increasing the temperature to 360K, which is above the melting temperature of PEO, 2mm bilayer LECs with PEO: KOTf concentrations of 100:1 and 200:1 were successfully turned on under constant bias voltage of 50V and 100V. EL was observed when p-doping and n-doping fronts met and formed a p-n junction. After the initial formation of the p-n junction, there was no obvious shift in the junction position. The images captured at peak current were displayed in Figure 7.1.

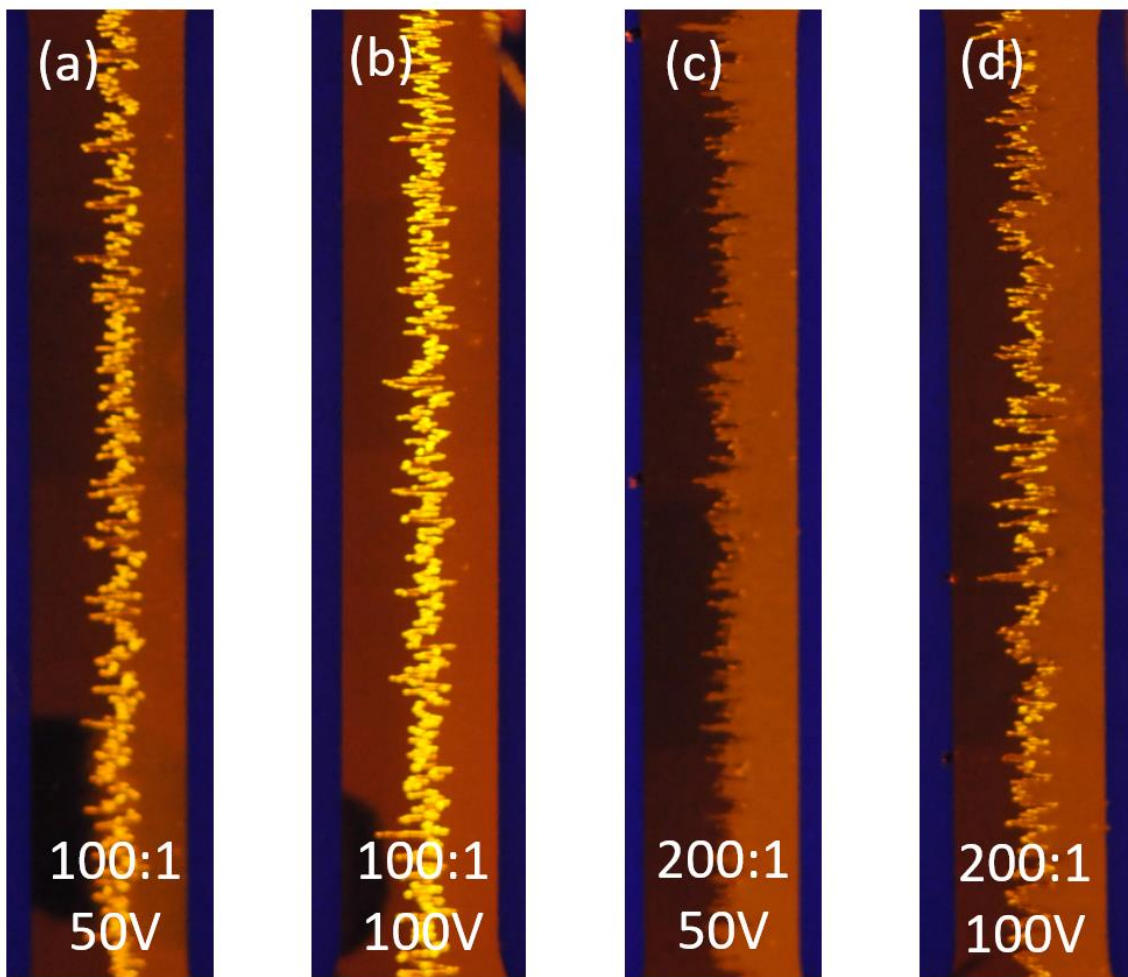


**Figure 7.1** Images captured at peak current for 2mm bilayer LECs devices with  
(a) PEO:KOTf concentration of 100:1 tested under a constant bias voltage of 50V  
(b) PEO:KOTf concentration of 100:1 tested under a constant bias voltage of 100V  
(c) PEO:KOTf concentration of 200:1 tested under a constant bias voltage of 50V

**(d) PEO:KOTf concentration of 200:1 tested under a constant bias voltage of 100V. All images are captured under the illumination of a 365nm UV ring light from above. All devices are tested under a constant temperature of 360K.**

The current vs. time characteristics were shown in Figure 7.2. The initial current and peak current for devices with different salt concentrations and tested under different bias voltages were presented in Table 7.1. Similar to bilayer LEC devices with higher salt concentrations, the cell current experienced a sharp rise when the furthest tips of p-doped and n-doped regions made contact. The initial junction formation times were extracted from the time-lapsed images and by fitting the current vs. time plot in the logarithm scale. The values determined by these two methods generally agreed and were presented in Table 7.1. The junction positions at peak current were analyzed from Figure 7.1 and presented in Table 7.1.

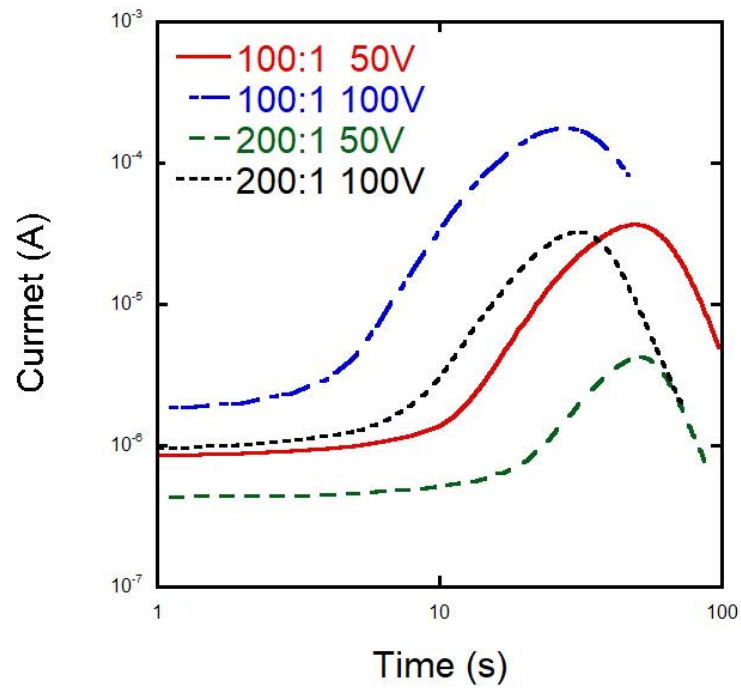


**Figure 7.2 Cell Current as a function of time for LEC devices with 100:1 and 200:1 PEO:KOTf concentration tested under a constant bias voltage of 50V and 100V and a constant temperature of 360K.**

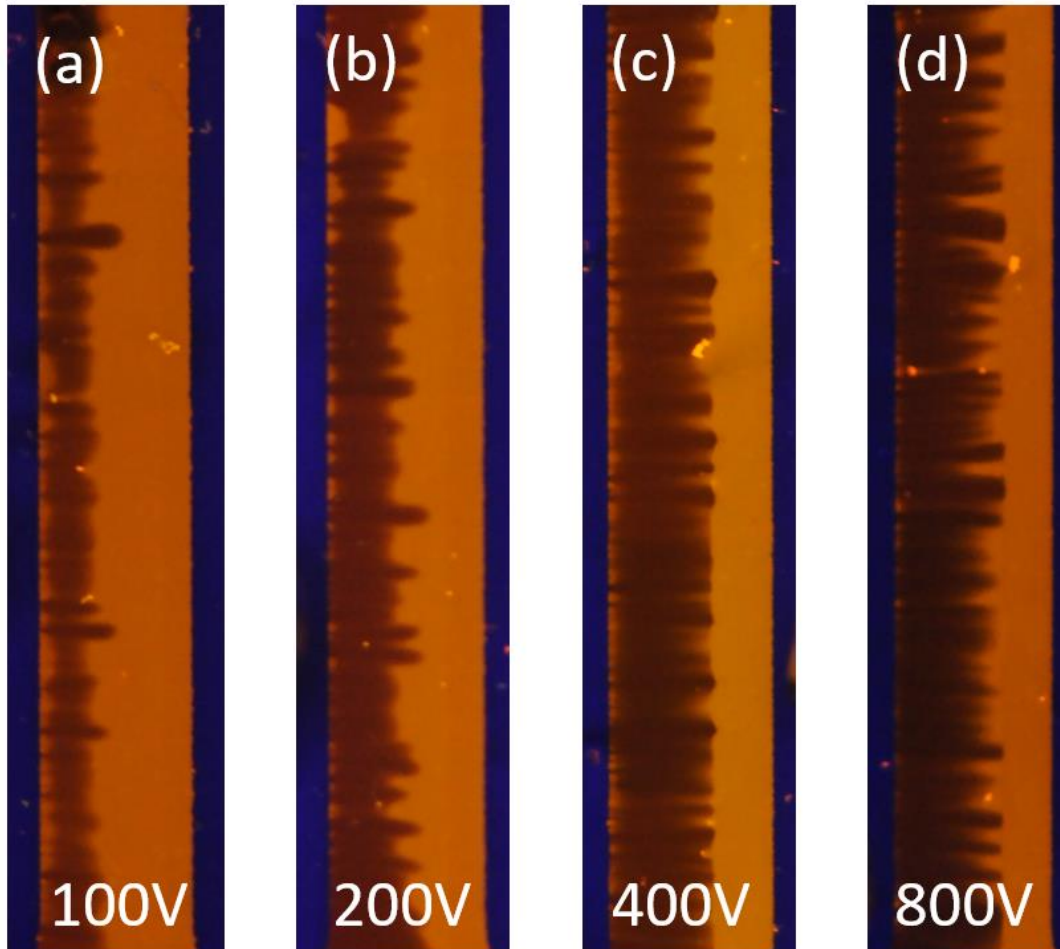
For bilayer LECs with a salt concentration of 100:1 and 200:1, by doubling the bias voltages, the initial current was increased by a factor of 2, which led to a faster doping propagation and a faster junction formation. Cells with lower salt concentration had a lower cell current and a longer junction formation time, which agreed with the effects of salt concentration studies in Chapter 4. Moreover, the junction position at peak current was found close to the cathode for devices with lower salt concentrations. The increase in bias voltages resulted in a junction position slightly closer to the anode and a more jagged junction.

PEO:KOTf Concentration (w/t %)	Bias Voltage (V)	Initial Current (nA)	Peak Current (nA)	Junction Formation Time (s)	Junction Position from the anode (mm)
100:1	50	847.90	36577	10 ± 2	1.087 ± 0.11
100:1	100	1737.00	176400	4 ± 1	1.047 ± 0.14
200:1	50	429.10	4211	16 ± 2	1.003 ± 0.09
200:1	100	962.40	32362	6 ± 1	1.000 ± 0.15

**Table 7.1 Initial current, peak current, junction formation time and junction position as a distance from the anode for bilayer LEC devices with different PEO:KOTf concentrations and tested under different bias voltage. The junction formation times were determined from current vs. time curves as described in Appendix A.**

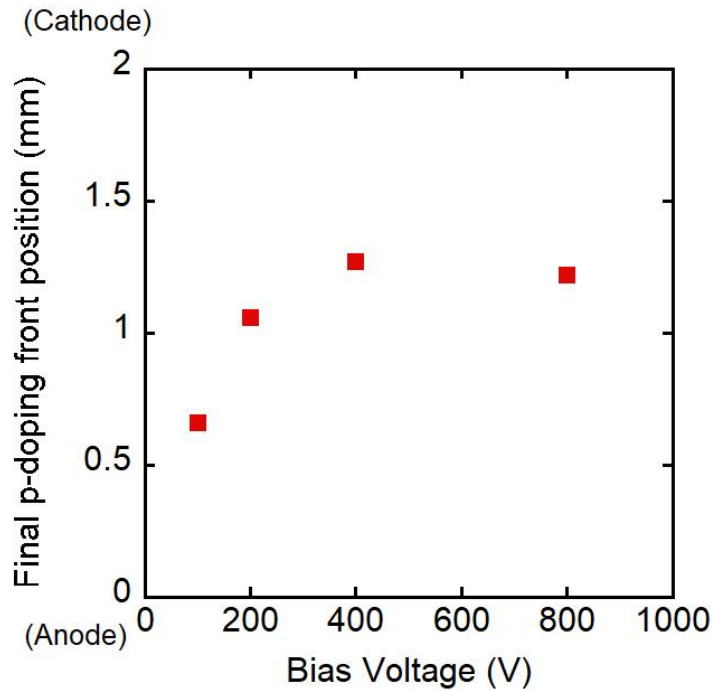
For devices with salt concentrations of 400:1, doping propagation was initiated as a constant bias voltage was applied, however, no EL was observed. Figure 7.3 shows the images captured once the doping propagation stopped. Under a constant bias voltage of

100V and 200V, doping propagation stopped before p-doped and n-doped regions made contact. Moreover, dedoping was observed at the p-doped regions close to the anode. As the bias voltage was increased to 400V, the p-doping front was pushed further toward the cathode. P-doping propagations stopped as p-doped and n-doped regions made contact with each other, however, no EL was observed. By increasing the bias voltage further to 800V, the dedoping effect close to the anode was eliminated, however, no EL was observed as the doping fronts met each other.



**Figure 7.3** Images captured once the doping propagation stopped for LECs devices with PEO: KOTf concentrations of 400:1 under a constant temperature of 360K and a constant bias voltage of (a) 100V (b) 200V (c) 400V (d) 800V.

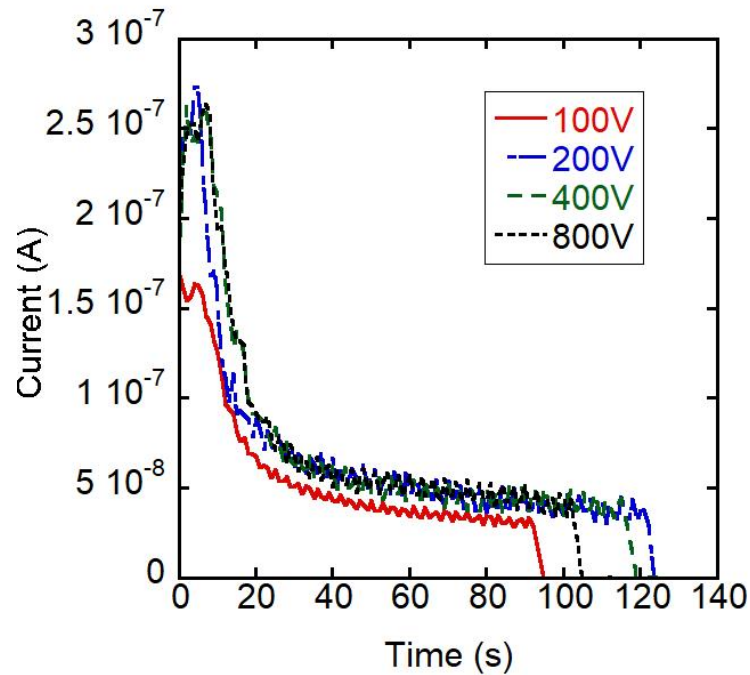
The average final p-doping position was extracted from Figure 7.3 and plotted in Figure 7.4. The final p-doping position was found proportional to the bias voltage at a lower bias voltage. By doubling the bias voltage from 100V to 200V, the average final p-doping front position was doubled. At a test condition of 400V or higher, a level off in the final p-doping position was observed, which means the p-doping propagation stopped once the p-doping front made contact with the n-doped region.



**Figure 7.4 Final p-doping front position relative to the anode as a function of bias voltage for 2mm bilayer LECs with PEO: KOTf concentration of 400:1.**

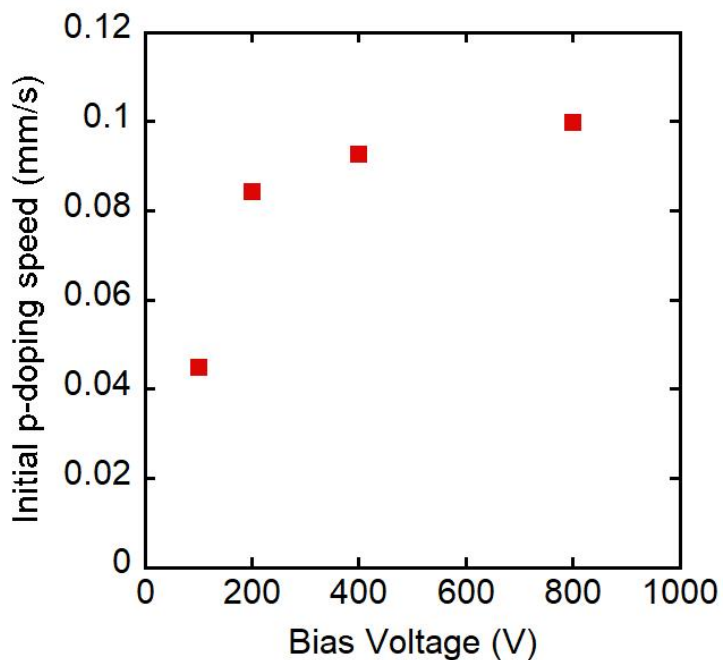
Figure 7.5 shows the current vs time characteristics for devices with a salt concentration of 400:1 tested under different constant bias voltages. Comparing the device tested under 200V to the same device tested under 100V, the initial current was about two times

higher. However, the current behavior was similar for devices tested under a bias voltage of 200V or higher. For all tests, the current experienced a slight rise immediately after applying the bias voltage. Doping propagation was initiated at the same time. As the current underwent an exponential drop, the doping propagation became slower and gradually stopped.



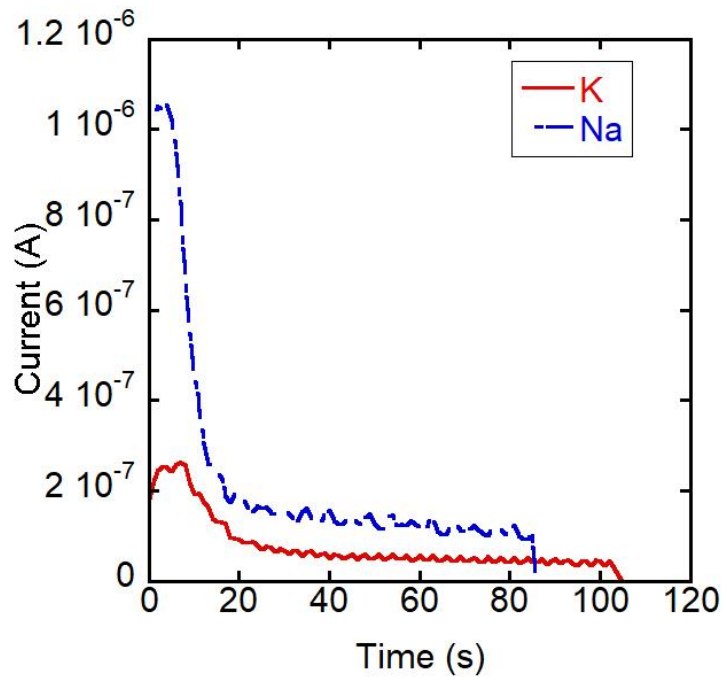
**Figure 7.5 Cell Current as a function of time for LEC devices with 400:1 PEO:KOTf concentration tested under different constant bias voltage and a constant temperature of 360K.**

Figure 7.6 shows the initial p-doping speed as a function of bias voltage for devices with salt concentrations of 400:1. The initial p-doping speed of the device tested under 200V was two times faster than the device tested under 100V. The initial p-doping speed was found proportional to the bias voltage, however, the increase in initial p-doping speed was less significant at higher bias voltage.



**Figure 7.6 Initial p-doping speed as a function of bias voltage for 2mm bilayer LECs with PEO: KOTf concentration of 400:1.**

From the results presented in Chapter 6, devices with sodium salt had fast doping propagation and higher cell current compared to devices with potassium salt, which means sodium salt had the potential to be turned on at low salt concentrations. Figure 7.7 compares the current vs time characteristics between the sodium salt device and potassium salt device. The initial current of the sodium salt device was 5 times higher than the potassium salt device, however, the current underwent an exponential drop, and no p-n junction was formed.



**Figure 7.7 Cell Current as a function of time for LEC devices with K and Na salts tested under a constant bias voltage of 800V and a constant temperature of 360K. The PEO:Salt concentrations were 400:1.**

Figure 7.8 shows the images captured after doping propagation stopped for potassium and sodium salt devices with 400:1 salt concentration. Despite the sodium salt device had a higher cell current, the doping propagation stopped before the n-doped and p-doped regions made contact. The final p-doping position of the sodium device is further away from the cathode compared to the potassium salt device.

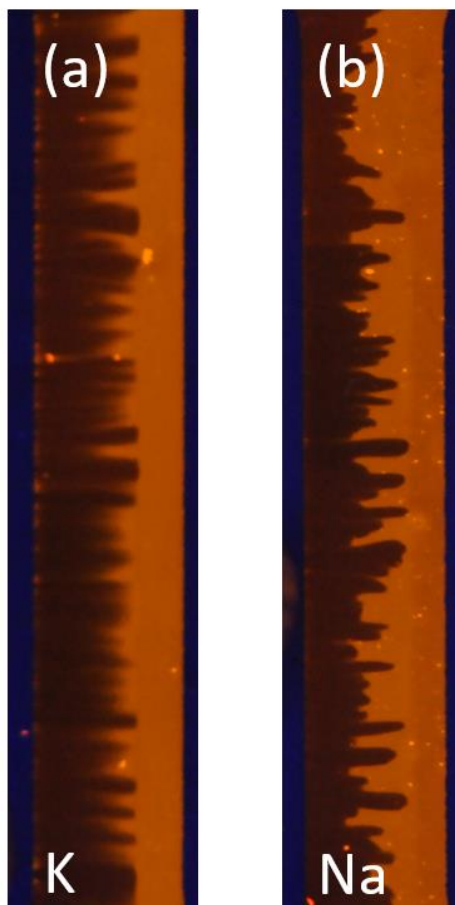


**Figure 7.8 Images captured once the doping propagation stopped for LECs devices with PEO: Salt concentrations of 400:1 under a constant temperature of 360K and a constant bias voltage of 800V. (a) Device with potassium salt. (b) Device with sodium salt.**

Single layer planar LECs had slower doping propagation and lower cell current compared to devices with bilayer structure. The lowest salt concentration single layer devices that were successfully turned on had a PEO: Salt concentration of 25:1. Figure 7.9 (a)-(c) shows the images captured at peak current for single layer LECs under different test conditions. Under a constant temperature of 330K, there was no increase in current or doping observed after applying a constant bias voltage of 25V. By increasing the

temperature to 360K, doping propagation was initiated, however, the p-n junction was not formed because the p-doped region and n-doping region did not make contact with each other. Higher bias voltage led to a faster doping propagation speed and pushed the doping front further toward the opposite electrode. Light emitting p-n junction was formed once the doping fronts met when 200V of constant bias voltage was applied. Planar LECs with bilayer structure, on the other hand, required lower temperature and bias voltage to be turned on. A bilayer device with the same salt concentration formed a continuous light emitting junction at peak current when a bias voltage of 25V was applied under a constant temperature of 330K.

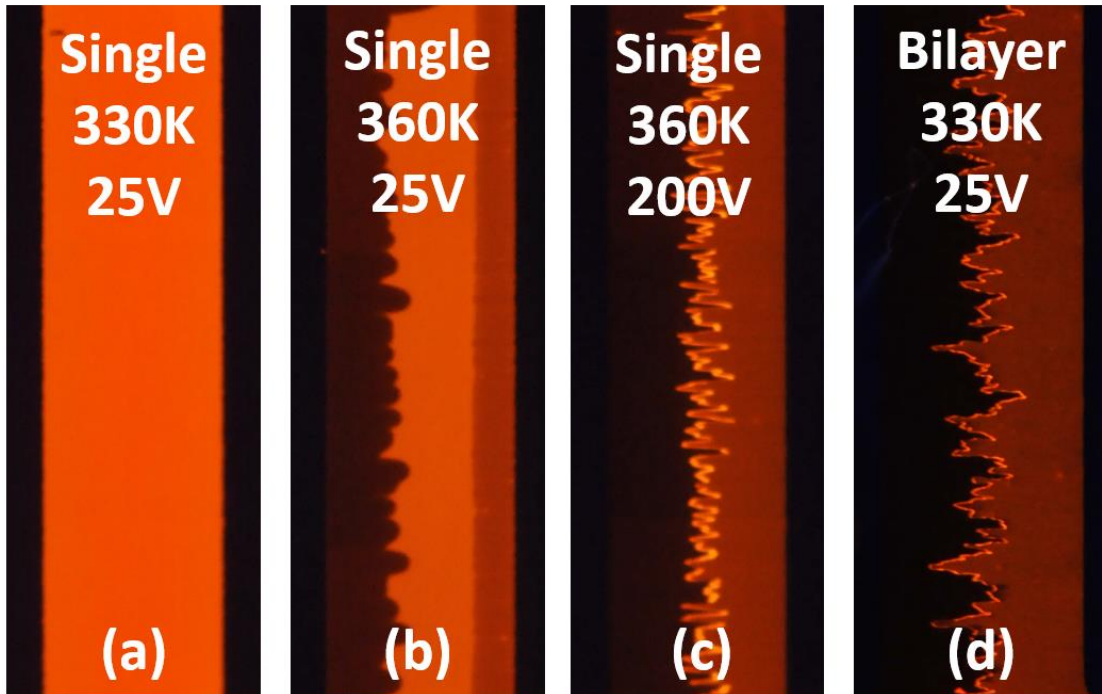


**Figure 7.9** Images captured at peak current for single layer and bilayer LEC devices with PEO: Salt concentrations of 25:1 (a) Single layer LEC tested under a constant temperature of 330K and a constant bias voltage of 25V (b) Single layer LEC tested under a constant temperature of 360K and a constant bias voltage of 25V. (c) Single layer LEC tested under a constant temperature of 360K and a constant bias voltage of 200V. (d) Bilayer LEC tested under a constant temperature of 330K and a constant bias voltage of 25V.

### 7.3 Conclusion

In this chapter, bilayer planar LECs with extremely low salt concentrations were presented and discussed. By increasing the temperature above the melting temperature of PEO, 2mm bilayer LECs with PEO: KOTf concentration of 200:1 was successfully turned on under a constant bias voltage of 50V. The junction position was approximately at the center of the 2mm gap size, and there is barely any shift in the junction position after its initial formation. The attempts to turn on devices with 400:1 salt concentration were not successful. The increase in bias voltage led to an increase in the cell current and doping propagation speed, which pushed the doping position further toward the opposite electrode. However, such an increase was less significant when the bias voltage went beyond 200V. Under a constant bias voltage of 800V, doping propagation stopped once the doping front made contact, however, no EL or any increase in cell current was observed. Devices with sodium salt had higher cell current compared to potassium salt devices, however, no EL was observed because p-doped and n-doped regions never made contact. In summary, 200:1 PEO: KOTf bilayer planar 2mm LEC was successfully turned on under a constant temperature of 360K and a constant bias voltage of 50V. For devices with lower salt concentrations, increasing the bias voltage led to a faster doping propagation and a larger doped region, however, no EL was observed in these devices. Mobile ions play critical roles in the operation characteristics of LECs. Once the doping of CP was initiated, mobile ions entered the CP layer and played a role of counter ions to compensate the injected electronic charges. For devices with extremely low salt concentrations, as the ions are used up by the doping process, the absence of ions in the

SPE lead to an increase in cell resistance, which led to a drop in cell current and stopped the formation of p-n junction.

## Chapter 8

### Conclusion

#### 8.1 Conclusion

In conclusion, I carried out four studies on bilayer planar LECs to investigate the effects of salt concentration, salt type, SPE layer thickness, and operating parameters. All devices were fabricated with an SPE underlayer and a MEH-PPV CP top layer. The interelectrode gap was 2mm for all devices. The planar LECs were tested under a constant bias voltage and a constant temperature inside a vacuum chamber. The doping propagation was visualized by capturing time-lapsed images under the illumination of a 365nm UV ring light from above, the cell current was measured simultaneously.

In the study on the effects of salt concentration, all devices were tested under a constant bias voltage of 25V and a constant temperature of 330K. Electrochemical doping and the light-emitting junction were observed for all devices with a salt concentration higher than 0.025. The salt concentration in the SPE had a strong effect on the cell current, doping propagation speed, and junction formation time, which proved direct evidence that the performance of the LECs was limited by the resistance of the SPE. In addition, after the initial junction formation, the junction position began to shift toward the cathode for cells with high salt concentrations. This effect is less significant for cells with lower salt concentrations. This behavior provided opportunities to improve device performance by controlling the position of the light emitting junction.

In the study on the effects of SPE layer thickness, electrochemical doping and light-emitting EL junction were observed for all devices with an SPE layer thickness between 770 nm and 30 nm. An SPE layer thinner than 500 nm led to a decrease in cell current

and doping propagation speed while increasing the SPE layer thickness beyond 500nm did not lead to any improvement in the cell performance. The position of the p-n junction is not thickness dependent. The results suggested that the conductance of the cells is proportional to the thickness of the SPE, which further proved that the performance of LECs was limited by the resistance of the SPE layer.

In the study on the cation type in the SPE, the effects of the size and the mass of cations in the SPE layer were visualized and investigated. For devices with alkali metal cations, the increase in the size of the cations result in a lower cell current, slower doping propagation speed, and a less significant shift of the junction position. Cells with lithium cations, however, behaved as an outlier due to local doping propagation. Cells with larger transition metal cations, on the other hand, required a higher temperature and bias voltage to turn on. Devices with Zn and Eu cations were successfully turned on; however, the junction positions were next to the cathode, and no n-doping was observed. The attempts to turn on devices with Terbium cations were not successful. Ammonium cations are similar in size compared to potassium cations, however, cell current, doping propagation speed, and junction position showed completely different behavior. Single layer planar LECs with different salts were tested and compared to bilayer devices, among all devices tested, bilayer devices always outperformance single layer devices. These results provided direct evidence that the type of cations has strong effects on the performance of LECs due to the change in ionic mobility, while ionic interlayer transportation was not the limiting factor.

In the study on extremely low salt concentration devices, cells with PEO: KOTf concentration as low as 200:1 were successfully turned on. The junction position was

approximately at the center of the 2mm gap size, and there is barely any shift in the junction position after its initial formation. Cells with lower salt concentrations did not have sufficient ions to form a light emitting p-n junction. The increase in bias voltage led to an increase in the cell current and doping propagation speed, which pushed the doping position further toward the opposite electrode. However, such improvement was less significant when the bias voltage went beyond 200V. Under high bias voltage, doping propagation stopped after the n-doped region made contact with the p-doped region, however, no junction formation was observed. These results suggested that in extreme low salt concentration devices, as mobile ions were used up in the doping process, the cells were highly resistive which did not provide sufficient current for junction formation.

## 8.2 Future Work

The studies in this thesis provided direct evidence that the performance of bilayer LECs is limited by the resistance of the SPE underlayer. The conductivity of the SPE can be improved by increasing the salt concentration or using salts with smaller cation sizes, however, such changes typically lead to a junction shift toward the cathode. The bilayer LECs have the unique advantage to visualize the effects of the SPE layer using highly sensitive imaging techniques. To further improve the performance of the LECs, the conductivity of the SPE can be improved by introducing nanoparticles into the SPE. Firstly, TiO<sub>2</sub> nanoparticles can be dissolved with PEO and salt in common solvent acetonitrile. The maximum ionic conductivity was found with an 8% TiO<sub>2</sub> nanofiller in the electrolyte. [48] In addition to nanofillers, an organic compound such as ethylene carbonate plays the role of plasticizer in a solid-state electrolyte. For an electrolyte system consisting of 20% (in wt%) EC, the conductivity was improved three times higher in magnitude. [49] Moreover, polypropylene carbonate because of its low degree of crystallinity, has the potential to improve the conductivity of the SPE. [50] However, because of the thermoplastic properties of PPC, the increase in conductivity is less significant at higher temperatures (>50°C) and gives the electrolyte fluidity at elevated temperatures. [51] The introduction of these compounds to the SPE has the potential to improve the performance of LECs and to turn on devices with lower salt concentrations. In Chapter 6, the effects of cations in a single layer and bilayer planar LECs were studied and compared. Among all the devices tested, the bilayer structure always outperformed single layer devices, which suggested that the size of voids in CP is greater than the size of the ions, and the interlayer ionic transport did not bring any limitations to the bilayer

devices. To expand on the studies on ionic effects, salts with different anions could be utilized in the SPE. By increasing the size of ions in the SPE, the limitation of the interlayer ionic transport could be studied.

## Appendix A

### Finding Junction Formation Time

#### Method 1: Time-Lapsed Images

The initial junction formation time can be determined from visually investigating the time-lapsed images by determining the time when the furthest tips of p-doping and n-doping fronts made contact. For example, Figure A.1 shows two continuous time-lapsed images capture at  $t = 12\text{s}$  and  $t = 15\text{s}$ . The time-lapsed images were captured with a time interval of 3 seconds. At  $t = 12\text{s}$ , p-doped and n-doped region did not make contact. The image captured at 15 second was determined as the first image which observed the contact between the furthest p-doping and n-doping tips. Therefore, the initial junction formation time for this device was determined as  $15 \pm 3$  seconds.

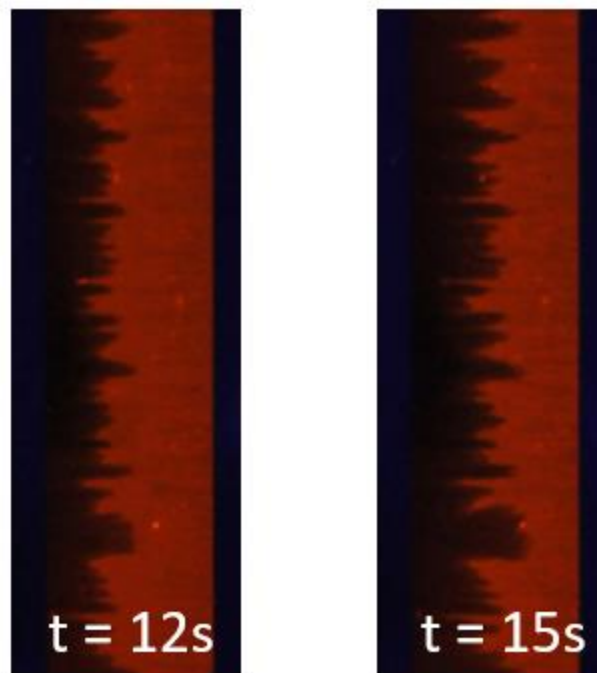


**Figure A.1** Example of two continuous time-lapsed images captured under the illumination of a 365nm UV ring light from above.

## Method 2: Fitting Current vs. Time Curve

Upon the formation of p-n junction, the cell current underwent a sharp rise due to the flow of electronic charges. The junction formation time can be determined from current vs. time curve by identifying the initial time of the sharp rise. As shown in Figure A.2, the initial current increase was fitted in red curve, while the sharp rise in current after junction formation was fitted in blue curve. The initial junction formation time was found as the interception of these two curves.

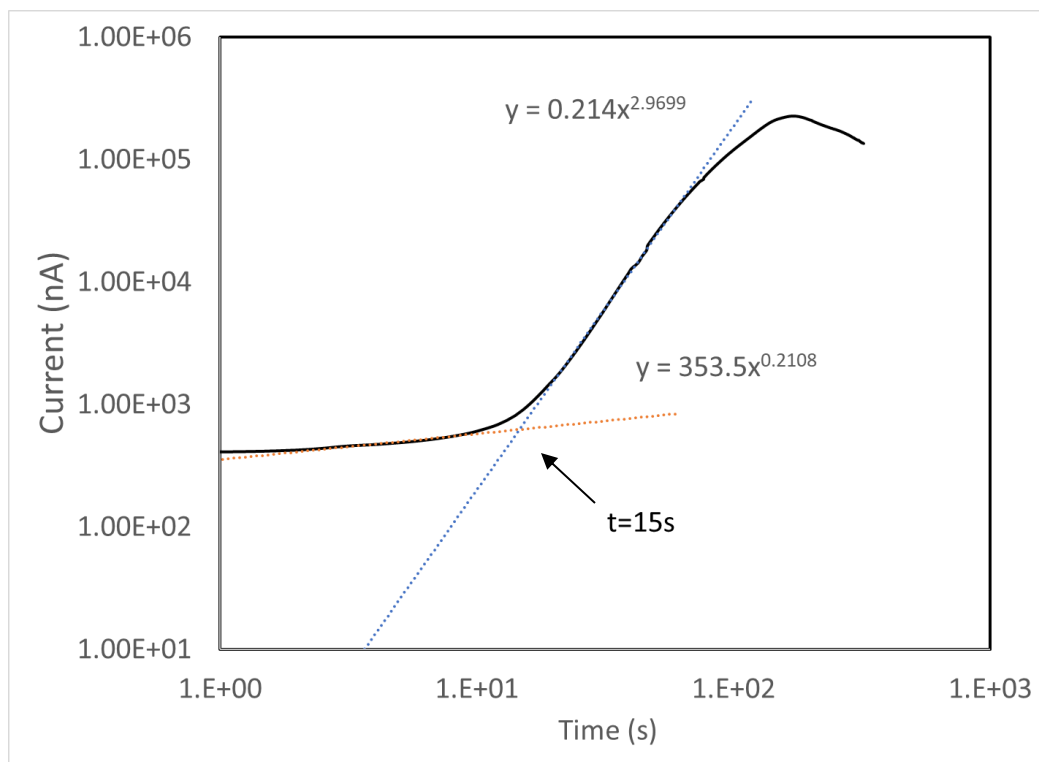


**Figure A.2 Example of finding the initial junction formation time from current vs. time plot.**

## Appendix B

### Finding Average p-doping Speed

Before the junction formation, p-doping propagated toward the cathode at a constant speed. The average p-doping position can be extracted from the time-lapsed images. As shown in Figure B.1, the average p-doping speed was determined by linear fitting the relationship between average p-doping front position and time.

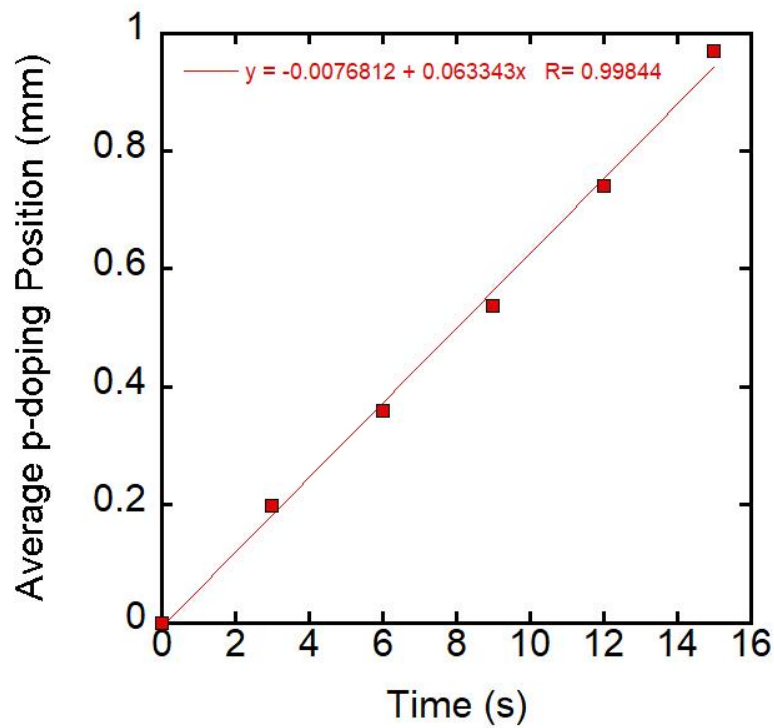


**Figure B.1** Example of linear fitting the relationship between the average p-doping position and time.

## References

- [1] H. Round, *Electr. World* 9 (1907) 309.
- [2] Krasnov, A. N. *Electroluminescent Displays: History and Lessons Learned. Displays* 2003, 24 (2), 73–79.
- [3] G. Destriau, *J. Chem. Phys.* 33 (1936) 587.
- [4] Bernanose, A. *Electroluminescence of Organic Compounds. British journal of applied physics* 1955, 6 (S4), S54–S55.
- [5] TANG, C. W.; VANSLYKE, S. A. *Organic Electroluminescent Diodes. Applied physics letters* 1987, 51 (12), 913–915.
- [6] Burroughes, J. H.; Bradley, D. D. C.; Brown, A. R.; Marks, R. N.; Mackay, K.; Friend, R. H.; Burns, P. L.; Holmes, A. B. *Light-Emitting Diodes Based on Conjugated Polymers. Nature (London)* 1990, 347 (6293), 539–541.
- [7] Pei, Q.; Yu, G.; Zhang, C.; Yang, Y.; Heeger, A. J. *Polymer Light-Emitting Electrochemical Cells. Science (American Association for the Advancement of Science)* 1995, 269 (5227), 1086–1088.
- [8] A. Asadpoordarvish, A. Sandström, C. Larsen, R. Bollström, M. Toivakka, R. Österbacka, L. Edman, *Adv. Funct. Mater.* 25, 3238 (2015).
- [9] A. Sandström, A. Asadpoordarvish, J. Enevold, L. Edman, *Adv. Mater.* 26, 4975 (2014).
- [10] A. Sandström, L. Edman, *Energy Technol.* 3, 329 (2015)
- [11] Pei, Q. B.; Yang, Y. *Efficient Photoluminescence and Electroluminescence from a Soluble Polyfluorene. J. Am. Chem. Soc.* 1996, 118, 7416–7417.

- [12] Kanagaraj, S.; Puthanveedu, A.; Choe, Y. Small Molecules in Light-Emitting Electrochemical Cells: Promising Light-Emitting Materials. *Adv. Funct. Mater.* 2020, 30, No. 1907126.
- [13] Fresta, E.; Costa, R. D. Beyond Traditional Light-emitting Electrochemical Cells - a Review of New Device Designs and Emitters. *J. Mater. Chem. C* 2017, 5, 5643–5675.
- [14] Gao, J.; Dane, J. Planar Polymer Light-Emitting Electrochemical Cells with Extremely Large Interelectrode Spacing. *Appl. Phys. Lett.* 2003, 83, 3027–3029.
- [15] Gao, J. Polymer Light-Emitting Electrochemical Cells-Recent Advances and Future Trends. *Curr. Opin. Electrochem.* 2018, 7, 87–94.
- [16] Hu, S.; Gao, J. Polymer Light-Emitting Electrochemical Cells with Bipolar Electrode-Dynamic Doping and Wireless Electroluminescence. *Adv. Funct. Mater.* 2020, 30, No. 1907003.
- [17] Alem, S.; Gao, J. The Effect of Annealing/Quenching on the Performance of Polymer Light-Emitting Electrochemical Cells. *Org. Electron.* 2008, 9, 347–354.
- [18] Cao, Y.; Yu, G.; Heeger, A. J.; Yang, C. Y. Efficient, Fast Response Light-Emitting Electrochemical Cells: Electroluminescent and Solid Electrolyte Polymers with Interpenetrating Network Morphology. *Appl. Phys. Lett.* 1996, 68, 3218–3220.

- [19] Cao, Y.; Pei, Q. B.; Andersson, M. R.; Yu, G.; Heeger, A. J. Light-Emitting Electrochemical Cells with Crown Ether as Solid Electrolyte. *J. Electrochem. Soc.* 1997, 144, L317–L320.
- [20] Sakanoue, T.; Yonekawa, F.; Albrecht, K.; Yamamoto, K.; Takenobu, T. An Ionic Liquid That Dissolves Semiconducting Polymers: A Promising Electrolyte for Bright, Efficient, and Stable Light-Emitting Electrochemical Cells. *Chem. Mat.* 2017, 29, 6122–6129.
- [21] Yang, Y.; Pei, Q. B. Efficient Blue-Green and White Light-Emitting Electrochemical Cells Based On Poly 9,9-bis(3,6-dioxaheptyl)-fluorene-2,7-diyl. *J. Appl. Phys.* 1997, 81, 3294–3298.
- [22] He, G.; Yang, C. H.; Wang, R. Q.; Li, Y. F. Light-Emitting Electrochemical Cells Based On Poly(2-methoxy-5-triethoxy-1,4-phenylene vinylene). *Displays* 2000, 21, 69–72.
- [23] Morgado, J.; Friend, R. H.; Cacialli, F.; Chuah, B. S.; Rost, H.; Moratti, S. C.; Holmes, A. B. Light-Emitting Electrochemical Cells Based On Poly(p-phenylene vinylene) Copolymers With Ion-Transporting Side Groups. *Synth. Met.* 2001, 122, 111–113.
- [24] Costa, R. D.; Orti, E.; Bolink, H. J.; Monti, F.; Accorsi, G.; Armaroli, N. Luminescent Ionic Transition-Metal Complexes for Light-Emitting Electrochemical Cells. *Angew. Chem., Int. Ed.* 2012, 51, 8178–8211.
- [25] Sessolo, M.; Tordera, D.; Bolink, H. J. Ionic Iridium Complex and Conjugated Polymer Used To Solution-Process a Bilayer White Light-Emitting Diode. *ACS Appl. Mater. Interfaces* 2013, 5, 630–634.

- [26] Shen, Y. L.; Kuddes, D. D.; Naquin, C. A.; Hesterberg, T. W.; Kusmierz, C.; Holliday, B. J.; Slinker, J. D. Improving Light-Emitting Electrochemical Cells With Ionic Additives. *Appl. Phys. Lett.* 2013, 102, 5.
- [27] Bastatas, L. D.; Lin, K. Y.; Moore, M. D.; Suhr, K. J.; Bowler, M. H.; Shen, Y. L.; Holliday, B. J.; Slinker, J. D. Discerning the Impact of a Lithium Salt Additive in Thin-Film Light-Emitting Electrochemical Cells with Electrochemical Impedance Spectroscopy. *Langmuir* 2016, 32, 9468–9474.
- [28] Suhr, K. J.; Bastatas, L. D.; Shen, Y. L.; Mitchell, L. A.; Holliday, B. J.; Slinker, J. D. Enhanced Luminance of Electrochemical Cells with a Rationally Designed Ionic Iridium Complex and an Ionic Additive. *ACS Appl. Mater. Interfaces* 2016, 8, 8888–8892.
- [29] Gautier, B.; Gao, J. Polymer Light-Emitting Devices Based on a Ppolymer/Salt Mixture. *Appl. Phys. Lett.* 2012, 101, No. 093302.
- [30] Gautier, B.; Wu, X. M.; Altal, F.; Chen, S. L.; Gao, J. Reverse Bias Activation of Salt-Doped Polymer Light-Emitting Devices. *Org. Electron.* 2016, 28, 47–52.
- [31] Sandstrom, A.; Matyba, P.; Inganas, O.; Edman, L. Separating Ion and Electron Transport: The Bilayer Light-Emitting Electrochemical Cell. *J. Am. Chem. Soc.* 2010, 132, 6646–6647.
- [32] Birdee, K., Hu, S., & Gao, J. (2020). Strong Doping and Electroluminescence Realized by Fast Ion Transport through a Planar Polymer/Polymer Interface in Bilayer Light-Emitting Electrochemical Cells. *ACS Applied Materials & Interfaces*, 12(41), 46381–46389.

- [33] van Reenen, S., Matyba, P., Dzwilewski, A., Janssen, R. A. J., Edman, L., & Kemerink, M. (2011). Salt concentration effects in planar light-emitting electrochemical cells. *Advanced Functional Materials*, 21(10), 1795–1802.
- [34] Fang, J., Yang, Y., & Edman, L. (2008). Understanding the operation of light-emitting electrochemical cells. *Applied Physics Letters*, 93(6).
- [35] Gao, J. Strategies Toward Long-Life Light-Emitting Electrochemical Cells. *ChemPlusChem* 2018, 83, 183–196.
- [36] Fang, J. F.; Matyba, P.; Edman, L. The Design and Realization of Flexible, Long-Lived Light-Emitting Electrochemical Cells. *Adv. Funct. Mater.* 2009, 19, 2671–2676.
- [37] Mardegan, L.; Dreessen, C.; Sessolo, M.; Tordera, D.; Bolink, H. J. Stable Light-Emitting Electrochemical Cells Using Hyperbranched Polymer Electrolyte. *Advanced functional materials* 2021, 31 (42), 2104249.
- [38] Hu, S.; Yeh, H.-W.; Gao, J. Polymer Light-Emitting Electrochemical Cells with Ultralow Salt Content: Performance Enhancement through Synergetic Chemical and Electrochemical Doping Actions. *Materials chemistry frontiers* 2021, 5 (4), 1847–1852.
- [39] Fang, J., Yang, Y., & Edman, L. (2008). Understanding the operation of light-emitting electrochemical cells. *Applied Physics Letters*, 93(6).
- [40] van Reenen, S., Matyba, P., Dzwilewski, A., Janssen, R. A. J., Edman, L., & Kemerink, M. (2011). Salt concentration effects in planar light-emitting electrochemical cells. *Advanced Functional Materials*, 21(10), 1795–1802.

- [41] Birdee, K.; Hu, S.; Gao, J. Strong Doping and Electroluminescence Realized by Fast Ion Transport through a Planar Polymer/Polymer Interface in Bilayer Light-Emitting Electrochemical Cells. *ACS applied materials & interfaces* 2020, 12 (41), 46381–46389.
- [42] J.R. Maccallum, A.S. Tomlin, C.A. Vincent, An investigation of the conducting species in polymer electrolytes, *Eur. Polym. J.* 22 (1986) 787–791.
- [43] Lascaud, S.; Perrier, M.; Vallee, A.; Besner, S.; Prud'Homme, J.; Armand, M. Phase Diagrams and Conductivity Behavior of Poly-(Rethylene Oxide)-Molten Salt Rubbery Electrolytes. *Macromolecules* 1994, 27, 7469–7477
- [44] F.M. Gray, Conductance and conducting species in amorphous polyether lithium perchlorate systems at very low salt concentration, *Solid State Ionics* 40-1 (1990) 637–640.
- [45] Bhattacharya, B., Lee, J. Y., Geng, J., Jung, H. T., & Park, J. K. (2009). Effect of cation size on solid polymer electrolyte based dye-sensitized solar cells. *Langmuir*, 25(5), 3276–3281.
- [46] Hu, Y.; Gao, J. Cationic Effects in Polymer Light-Emitting Electrochemical Cells. *Applied physics letters* 2006, 89 (25), 253514–253514–3.
- [47] Hu, S.; Yeh, H.-W.; Gao, J. Polymer Light-Emitting Electrochemical Cells with Ultralow Salt Content: Performance Enhancement through Synergetic Chemical and Electrochemical Doping Actions. *Materials chemistry frontiers* 2021, 5 (4), 1847–1852.
- [48] Polu, A. R.; Rhee, H.-W. Effect of TiO<sub>2</sub> Nanoparticles on Structural, Thermal, Mechanical and Ionic Conductivity Studies of PEO<sub>12</sub>-LiTDI Solid Polymer

Electrolyte. *Journal of industrial and engineering chemistry* (Seoul, Korea) 2016, 37, 347–353.

- [49] Johan, M. R.; Shy, O. H.; Ibrahim, S.; Mohd Yassin, S. M.; Hui, T. Y. Effects of Al<sub>2</sub>O<sub>3</sub> Nanofiller and EC Plasticizer on the Ionic Conductivity Enhancement of Solid PEO–LiCF<sub>3</sub>SO<sub>3</sub> Solid Polymer Electrolyte. *Solid state ionics* 2011, 196 (1), 41–47.
- [50] Yang, H.; Zhang, Y.; Tennenbaum, M. J.; Althouse, Z.; Ma, Y.; He, Y.; Wu, Y.; Wu, T.-H.; Mathur, A.; Chen, P.; Huang, Y.; Fernandez-Nieves, A.; Kohl, P. A.; Liu, N. Polypropylene Carbonate-Based Adaptive Buffer Layer for Stable Interfaces of Solid Polymer Lithium Metal Batteries. *ACS applied materials & interfaces* 2019, 11 (31), 27906–27912.
- [51] Zhang, J.; Zhao, J.; Yue, L.; Wang, Q.; Chai, J.; Liu, Z.; Zhou, X.; Li, H.; Guo, Y.; Cui, G.; Chen, L. Safety-Reinforced Poly- (Propylene Carbonate)-Based All-Solid-State Polymer Electrolyte for Ambient-Temperature Solid Polymer Lithium Batteries. *Adv. Energy Mater.* 2015, 5, 1501082.